# REPORT DOCUMENTATION PAGE

*Form Approved*
*OMB No. 0704-0188*



| **1. REPORT DATE** *(DD-MM-YYYY)* | **2. REPORT TYPE** | **3. DATES COVERED** *(From - To)* |
|---|---|---|
| 30-09-2018 | Final | Apr 4, 2018 - Sept 30, 2018 |

**4. TITLE AND SUBTITLE**
Analysis and Prediction of Sea Ice Evolution
using Koopman Mode Decomposition Techniques

**5a. CONTRACT NUMBER**
N00014-18-P-2004

**5b. GRANT NUMBER**

**5c. PROGRAM ELEMENT NUMBER**

**6. AUTHOR(S)**
Maria Fonoberova, Igor Mezic, James Hogg

**5d. PROJECT NUMBER**

**5e. TASK NUMBER**

**5f. WORK UNIT NUMBER**

**7. PERFORMING ORGANIZATION NAME(S) AND ADDRESS(ES)**
AIMdyn, Inc.
1919 State St., Ste. 207
Santa Barbara, CA 93101

**8. PERFORMING ORGANIZATION REPORT NUMBER**
ONR-Final-2018

**9. SPONSORING / MONITORING AGENCY NAME(S) AND ADDRESS(ES)**
Office of Naval Research
875 N. Randolph St.
Arlington, VA 22201

**10. SPONSOR/MONITOR'S ACRONYM(S)**

**11. SPONSOR/MONITOR'S REPORT NUMBER(S)**

**12. DISTRIBUTION / AVAILABILITY STATEMENT**
Freely Available

**13. SUPPLEMENTARY NOTES**

**14. ABSTRACT**
Koopman Mode Decomposition (KMD) was applied to satellite data of sea ice concentration and thickness for the northern and southern hemispheres to gain insight into the temporal and spatial dynamics of the sea ice behavior and to predict future sea ice behavior. Primary results were the possible change in sea ice dynamics in the 1990's, based on examination of Koopman eigenvalue distributions; the geographic change in sea ice concentration over time, specifically the reduction in mean sea ice concentration and annual variation off of West Antarctica; and prediction of sea ice concentration several years in the future using Koopman reconstruction techniques.

**15. SUBJECT TERMS**
Koopman Mode Decomposition, sea ice concentration, sea ice thickness, northern and southern hemispheres, prediction of the future sea ice behavior

| **16. SECURITY CLASSIFICATION OF:** | | | **17. LIMITATION OF ABSTRACT** | **18. NUMBER OF PAGES** | **19a. NAME OF RESPONSIBLE PERSON** |
|---|---|---|---|---|---|
| **a. REPORT** | **b. ABSTRACT** | **c. THIS PAGE** | | | Maria Fonoberova |
| None | None | None | None | 30 | **19b. TELEPHONE NUMBER** *(include area code)* 805-687-6999 |

# Final Technical Report

# Abstract

Koopman Mode Decomposition (KMD) was applied to satellite data of sea ice concentration and thickness for the northern and southern hemispheres to gain insight into the temporal and spatial dynamics of the sea ice behavior and to predict future sea ice behavior. Primary results were the possible change in sea ice dynamics in the 1990's, based on examination of Koopman eigenvalue distributions; the geographic change in sea ice concentration over time, specifically the reduction in mean sea ice concentration and annual variation off of West Antarctica; and prediction of sea ice concentration several years in the future using Koopman reconstruction techniques.

# Accomplishments

## Summary

Koopman Mode Decomposition (KMD) was applied to satellite data of sea ice concentration and thickness for the northern and southern hemispheres to gain insight into the temporal and spatial dynamics of the sea ice behavior and to predict future sea ice behavior. Primary results were the possible change in sea ice dynamics in the 1990's, based on examination of Koopman eigenvalue distributions; the geographic change in sea ice concentration over time, specifically the reduction in mean sea ice concentration and annual variation off of West Antarctica; and prediction of sea ice concentration several years in the future using Koopman reconstruction techniques.

## Introduction

Sea ice is floating ice that forms when ocean water freezes. The formation and distribution of sea ice plays an important role in the planet's climate and thus large amounts of data related to quantitative measures of sea ice have been collected, including continuous satellite remote sensing measurements since 1979. The decreasing extent of Arctic sea ice over the last several decades has had negative effects on Arctic wildlife and local communities, while also potentially opening new regions to maritime commerce and natural resources exploration. The future of sea ice behavior is thus of great significance for environmental, economic, and national security reasons.

Koopman Mode Decomposition (KMD) is a mathematical tool well suited to analyzing sea ice dynamical behavior because it identifies important spatial structures and their complex time dependence from large data sets such as those available for sea ice. The data set found to be most suitable for study and prediction with KMD is the satellite-based sea ice concentration measurements from the NSIDC Sea Ice Index, due primarily to the long and continuous time period (1979 to the present) and the large geographic regions over which this data is available. Sea ice thickness data from the CryoSat-2 satellite was also considered, but this data was less ideal for KMD processing because it is available for a shorter year

range (2011 to the present) than the concentration data and therefore the dynamics can only be investigated over commensurately short time periods.

The three primary results of the work are

1. The identification of possible new dynamics beginning in the 1990's based on examination of Koopman eigenvalue distributions, where significant growing or slowly decaying modes appear more commonly.

2. The presence of Koopman modes showing the change in geographic distribution of sea ice over the time period covered by satellite data, specifically the reduction in the mean antarctic sea ice concentration and the increased annual variation near West Antarctica.

3. The ability of Koopman-based reconstruction techniques to predict future sea ice behavior.

Applying the windowed time range Koopman mode analysis techniques and examination of the Koopman modes corresponding to the Koopman eigenvalues identified as being of interest. For each related eigenvalue and mode, the eigenvalue determines the time dependent behavior of the mode and the mode determines the spatial significance of the specific dynamical behavior given by the eigenvalue. In this case, examination of a mode shows the geographic locations where sea ice concentration is changing and the related eigenvalue tells how the concentration in those locations changes over time.

It was of interest to compare the previously processed sea ice concentration data results with a data set for a similar but distinct observable. Sea ice thickness is an appropriate observable to compare with, as sea ice thickness is expected to have broadly similar time dependence to sea ice concentration, but with the possibility of thickness variations occurring in regions where the concentration remains high. The available sea ice thickness satellite data does not cover as long a time period as the sea ice concentration (2011 onward vs. 1979 onward) but that temporal coverage is sufficient for comparison with the more recent concentration results. The sea ice thickness data required different preprocessing than the concentration data, but once properly preprocessed the same Koopman Mode Analysis approach could be applied to the thickness data as had been applied to the concentration data.

Koopman Mode Decomposition of a time-dependent signal into Koopman modes and eigenvalues permits reconstruction of the original signal, and also prediction of future values of the input signal beyond the time period used as an input to the KMD algorithm. In the case of sea ice measurements, it is of interest to predict the geographic distribution of observables of interest in future years.

Satellite measurements of sea ice concentration are available since 1979 and the work on this program demonstrated the usefulness of examining various length windows of this data to capture multiyear dynamics. This approach permits the use of Koopman reconstruction techniques to compare actual data with the predicted sea ice concentration values for all but the most recent data.

KMD reconstruction techniques were applied to the prediction of future sea ice concentrations in particular geographic regions. Because the dynamics of the seasonal variation in

sea ice concentration differ greatly between high latitude regions, which have nearly complete sea ice coverage in the winter and retain some sea ice through the summer, and lower latitude regions, which do not necessarily reach complete sea ice coverage in the winter and nor retain any sea ice through the summer, it is of interest to examine the KMD prediction results in particular geographic regions. To that end, the maps of the NSIDC Sea Ice Index for the northern and southern hemispheres were divided into approximate seas and other geographic regions (see Figures 1 and 2) and the KMD prediction results for each region were examined separately. These regions match those commonly used for the Antarctic by researchers, with the exception that traditionally the Amundsen and Bellingshausen Seas are combined into one region but here we split them into separate regions to expose any potential differences in their behavior.

The focus was visualizing the "goodness" of the KMD prediction results by comparison with actual sea ice concentration data for the time period the prediction was performed over.

Presentation of prediction results for a wide range of year windows and prediction years is desirable but presents a challenge in data visualization due to the dimensionality of the data (that is, there are prediction results for years between 1982 and 2017, where multiple predictions are made for each year from the different year window ranges from different numbers of years prior to the prediction year, and the character of the prediction can change with the season in each year). To produce the most useful and easily interpreted data visualization, it was decided to reduce the dimensionality of the results by only considering predictions one year in the future (e.g., for an input year range of 1979-1981, only the prediction for 1982 is shown), and instead of presenting results for all twelve months of the year in one figure, separate figures are shown for the two months of greatest interest: the month where the sea ice concentration is at a maximum (March in the northern hemisphere and September is in the southern hemisphere) and the month where the sea ice concentration is at a minimum (September in the northern hemisphere and February in the southern hemisphere). Examination of these extrema months can give a better sense of the usefulness of KMD techniques for predicting trends in the sea ice dynamics.

## Methods

The general data analysis method was to convert the image data files from the NSIDC Sea Ice Index of sea ice concentration or thickness showing average monthly concentration to numerical arrays, remove the pixels corresponding to land areas, and reshape the remaining sea pixels into a 1-D array for each month. For the concentration data, data files were missing for a small number (three in the northern hemisphere and two in the southern hemisphere) of months in the 1980's, so it was necessary to interpolate over the missing months of data to allow use of all data back to 1979, giving 39 full years of data (1979 to 2017). This sea ice thickness data was from the CryoSat-2 satellite and consisted of 30 day sliding averages of sea ice thickness for the period between late August and mid May beginning in the year 2011. In order to best compare the results with the sea ice concentration data, the considered data consisted of approximately monthly data starting on the first day of each month and beginning in January of each year. A "full" year of data therefore consisted of eight months and there were seven years of full data available (2011-2017).

The arrays for each month were then combined into a 2-D data matrix for performing

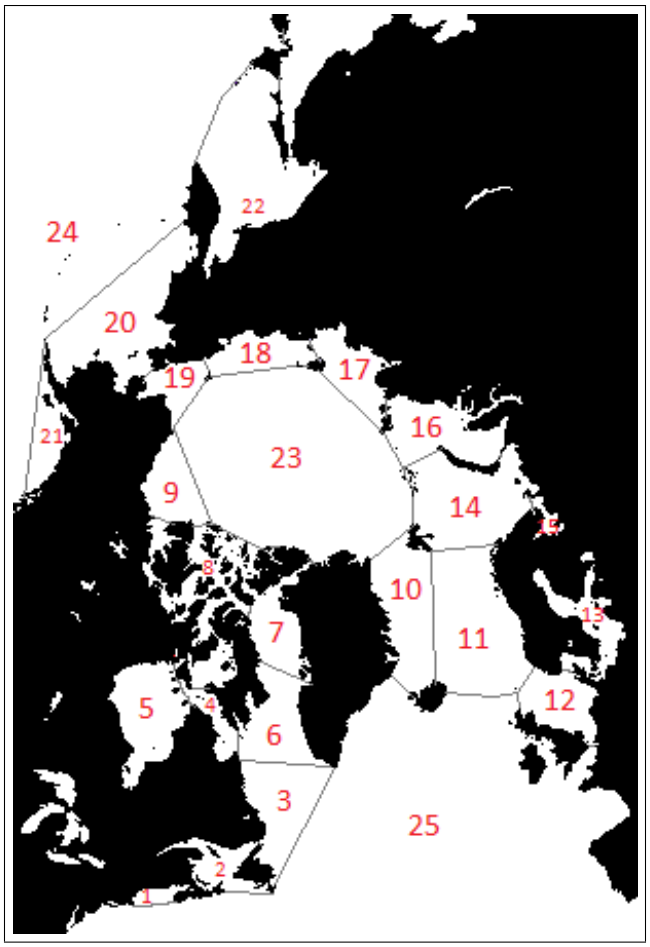


Figure 1: Northern hemisphere geographic regions considered in reconstruction results shown here. 1: Bay of Fundy, 2: Gulf of St Lawrence, 3: Labrador Sea, 4: Hudson Strait, 5: Hudson Bay, 6: Davis Strait, 7: Baffin Bay, 8: Northwestern Passages, 9: Beaufort Sea, 10: Greenland Sea, 11: Norwegian Sea, 12: North Sea, 13: Baltic Sea, 14: Barents Sea, 15: White Sea, 16: Kara Sea, 17: Laptev Sea, 18: East Siberian Sea, 19: Chukchi Sea, 20: Bering Sea, 21: Gulf of Alaska, 22: Sea of Okhotsk, 23: Arctic Ocean, 24: North Pacific Ocean, 25: North Atlantic Ocean.

KMD analysis run using multiple algorithms (Arnoldi, DMD RRR, iDMD, Arnoldi Vandermonde Cauchy RRD, and Arnoldi Vandermonde LDU). The resulting Koopman eigenvalues and mode spectra were examined and also used to perform prediction of future sea ice behavior using Koopman reconstruction techniques. It was found that different Koopman algorithms produced identical results, which was a strong indication that the results are a good representation of the true Koopman eigenvalues and modes.

To capture trends in the data that vary over relatively short time scales, the above analysis was performed on windowed data sets. The windowing consisted of performing KMD on subsets of the sea ice concentration data covering time periods of 3 to 39 years (e.g. five year windows consisted of 1979-1983, 1980-1984, . . . , 2013-2017), and for sea ice thickness three five-year windows between 2011 and 2017 and a single seven year window

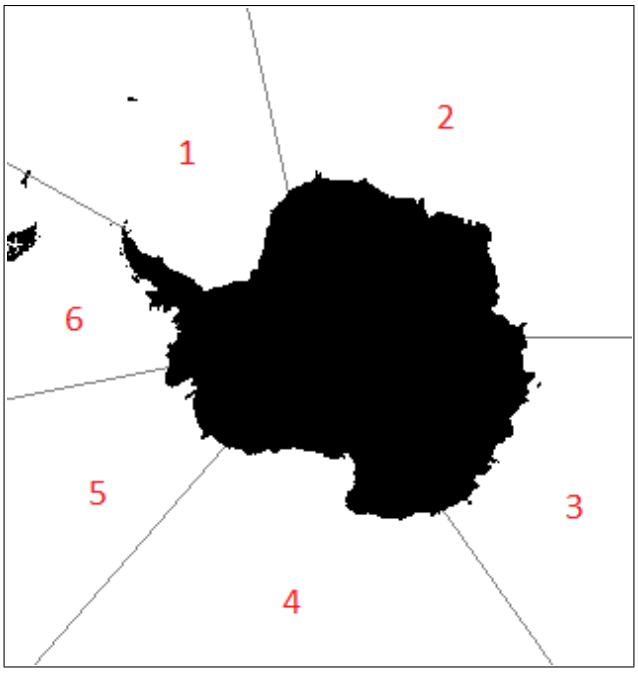


Figure 2: Southern hemisphere geographic regions considered in reconstruction results shown here. 1: Weddell Sea, 2: Indian Ocean, 3: West Pacific Ocean, 4: Ross Sea, 5: Amundsen Sea, 6: Bellingshausen Sea.

covering all of the available years.

The time dependence of a Koopman mode depends on the corresponding eigenvalue's real and imaginary components; the real component determines the growth or decay behavior, while the imaginary component determines the oscillatory behavior. To identify multiyear trends, the eigenvalues with oscillation periods longer than one year (i.e. small imaginary components) were selected and their related modes examined to see the geographic regions that experience the identified time dependent changes in sea ice concentration. The growth or decay behavior (determined by the real component) is also important in understanding the multiyear change in sea ice concentration, as a small (more negative) value implies a rapidly decaying trend, which if sufficiently fast is unlikely to be of long-term importance, while a larger (less negative) value corresponds to more gradual decay that can be of significance over multi-year time scales. Note that no eigenvalues with positive real components were found, consistent with the observed trend of decreasing sea ice concentration over time. The geographic information revealed in the modes was of interest to localize regions where sea ice thickness is changing the most.

Reconstruction of the $N_p$ sea ice concentration pixel values $\mathbf{C}$ at discrete time step $k$ is performed using the Koopman eigenvalues $\lambda_j$ and the Koopman modes $\mathbf{v}_j$ obtained from applying KMD to the concentration values over $N$ time steps (months, in this case):

$$\mathbf{C}_k = \sum_{j=1}^{N} \lambda_j^{k-1} \mathbf{v}_j$$

Here, there are $N$ Koopman eigenvalues and Koopman modes, where each Koopman eigen-

value is a single complex number and each Koopman mode has dimensions 1 by $N_p$.

For $1 \leq k \leq N$, $\mathbf{C_k}$ is termed a reconstruction of the $k$th time step in the original data $\mathbf{C}$, as the Koopman eigenvalues and modes came from a decomposition of the observations over this time range and should simply reproduce the data used as input to the KMD. For $k > N$, $\mathbf{C_k}$ is a prediction of the future behavior of the sea ice concentration for the (future) $k$th time step, based on the system dynamics deduced from decomposition of earlier observations.

KMD reconstruction was performed on all data from the given hemisphere, then the pixels corresponding to each region were identified and compared with actual data (when available). Note that an alternate approach, not shown here, is to apply KMD to only the data from a particular region and then perform reconstruction for that region using those KMD results. It was found that the predictions produced using only the data from a particular region were less accurate than predictions from applying KMD to the entire hemisphere of data, presumably due to the lower dimensionality of the former case.

Two methods were applied to visualize the "goodness" of the KMD reconstruction results. The first was based on a direct pixel-to-pixel comparison of the actual data and prediction results. In this case, the calculation consisted of, for each month and for each region, taking the mean of the absolute value of the difference between the actual data and prediction results for all pixel values for which either the actual data or prediction results contained a sea ice concentration value greater than zero. The reason for restricting consideration to nonzero concentration pixels was to avoid giving a misleading impression of the goodness of the prediction results, particularly when there is a large fraction of ice-free pixels in lower latitude regions and in the summer. The second visualization method was to plot the mean sea ice concentration value of the actual data and prediction results in each region. This approach does not judge the exact geographic precision of the prediction results but provides a broader sense of whether the predictions match the actual increase or decrease of sea ice in a particular region.

## Results and Discussion

A general result observed of performing KMD processing on the sea ice concentration data using the KMD algorithms listed above was that all of the algorithms gave identical or effectively identical outputs. This suggests that the sea ice concentration data dynamical behavior is "well behaved" in some sense, presumably that the resulting condition number is sufficiently small that any of the various approximations of the Koopman decomposition are valid here. This is a desirable result, as it supports the conclusion that the KMD results obtained here are physically meaningful and not numerical artifacts.

### Koopman Eigenvalues and Modes for Sea Ice Concentration

Specific observations from the windowed processing were:

1. The identification based on eigenvalue plots of the existence of growing or slowly decaying modes only intermittently before the 1990's and mostly consistently present from the 1990s onward. These were most visible in the five year window case and also visible in the ten year case (see Figures 3 and 5).

2. The existence of a consistent annual (i.e. period one year) signal as expected and, generally, consistent spectral results from year to year (see Figures 4 and 6).

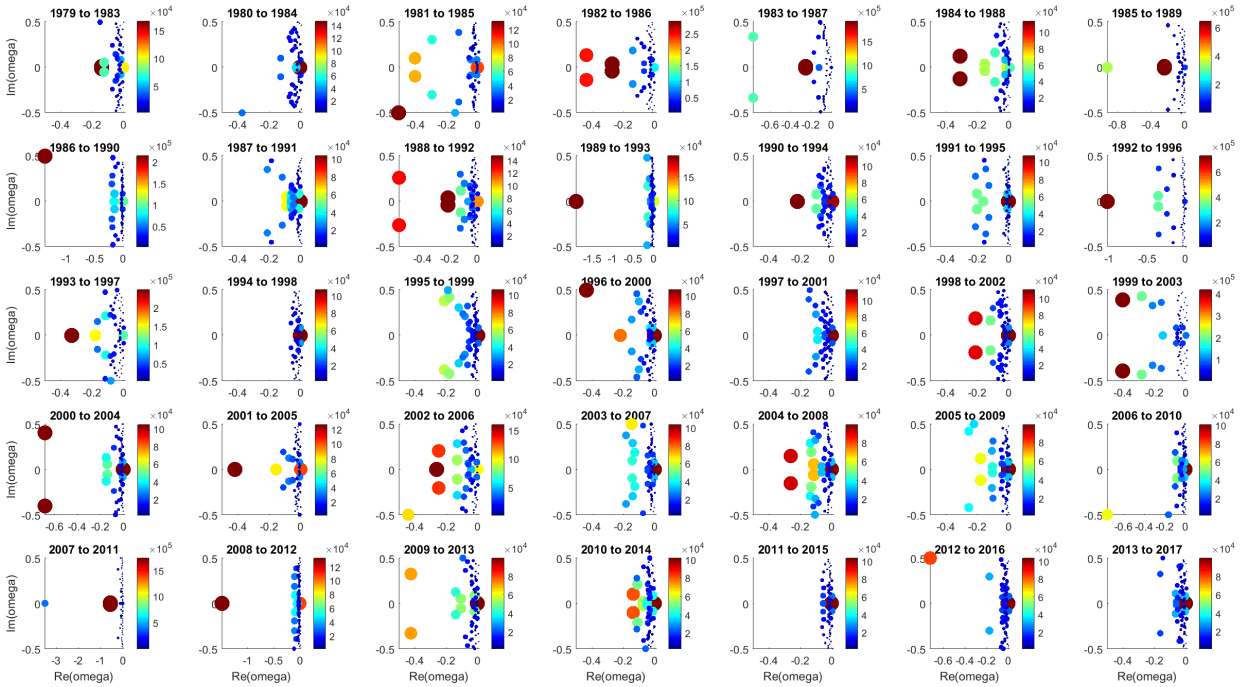


Figure 3: Northern hemisphere Koopman eigenvalues for 5 year time windows beginning in 1979. Each circle corresponds to the complex frequency of a Koopman mode, where the size and color of the circle are both representations of the L2 norm of the corresponding mode, the position along the horizontal axis shows the growth or decay constant of the mode (e.g. the more negative the value the faster the mode decays), and the position along the vertical axis shows the oscillatory frequency of the mode. The time scale is in months, so the two circles generally visible at approximately $\pm 0.08$ on the vertical axis are the expected annual variation of the sea ice concentration. The novel result apparent is the mostly consistent presence of a large norm mode near the origin beginning in the 1990-1994 window. This slowly decaying or growing mode suggests a change in sea ice dynamics beginning in the 1990's.

The eigenvalues for the five-year windowed analysis applied to the southern hemisphere sea ice concentration data show similar trends as the north hemisphere data. In Figure 5, it is seen that beginning in the 1990's, there is often one or more eigenvalues with imaginary values near zero and close to the origin, representing slowly decaying behavior (i.e. decreasing sea ice concentration). The spectrogram of the same eigenvalues (Figure 6) shows the expected peak at a period of one year (representing the annual sea ice variation), with generally increasing amplitude over time, representing a relatively greater annual variation in sea ice concentration.

As described above, the Koopman modes show the spatial significance of the dynamical behavior described by the eigenvalues. Figure 7 shows modes corresponding to the mean

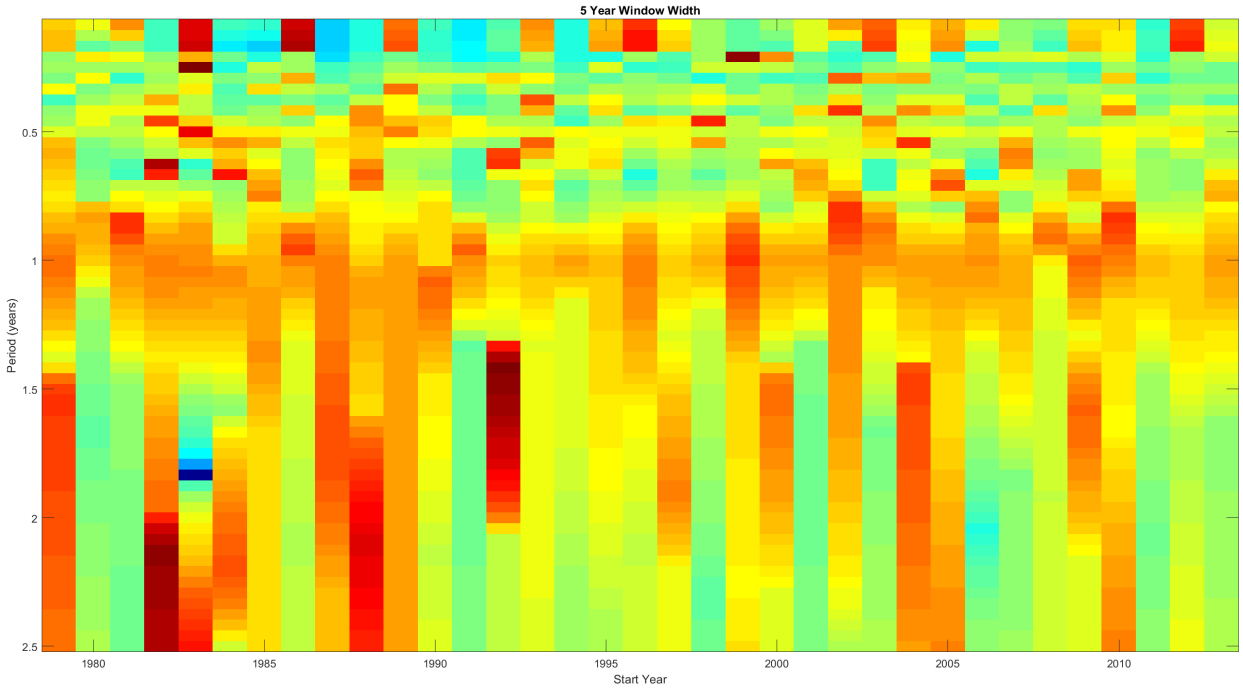


Figure 4: Spectrogram of the northern hemisphere Koopman mode spectra for 5 year time windows beginning in 1979. The period (in years) is shown here instead of frequency, because the multiyear dynamics are of greater interest than month-scale behavior. The expected annual cyclical behavior is clearly visible in each time window, and harmonics at two years are also apparent in many cases.

and annual variation in sea ice concentration for the southern hemisphere for the five year windows from 1979-1983 and 2013-2017. It is clear that the mean sea ice concentration is less in the later time period, suggesting that the sea ice does not reach as great an extent in the winter, and the annual variation occurs over a larger region closer to Antarctica, suggests a year-to-year reduction in summer sea ice concentration near the continent, particularly near West Antactica. Similarly, Figure 8 shows the modes corresponding to the mean and annual variation for sea ice concentration in the northern hemisphere for the two different year year periods. The same decrease in mean sea ice concentration and increase in the region undergoing significant annual variation is observed. Such changes are especially apparent in the regions of the Beaufort Sea north of Alaska and the Kara Sea north of Russia.

Analysis of the entire 39 year period covered by the data shows similar results as obtained from comparing the early and later five year periods. Figure 9 shows a mode with slow decay and long oscillation period representing a decrease in sea ice concentration in the southern hemisphere, primarily consisting of a decrease in sea ice concentration in West Antarctica. This region is known to be warming more rapidly than the region as a whole, so this KMD mode is consistent with that observation and the result from the five year windows above showing decreased mean ice concentration and increased annual variation near West Antarctica. Figure 10 shows a number of similar modes from the northern hemisphere for the entire 39 year data set with slowly decaying and, in some cases, slowly oscillating time

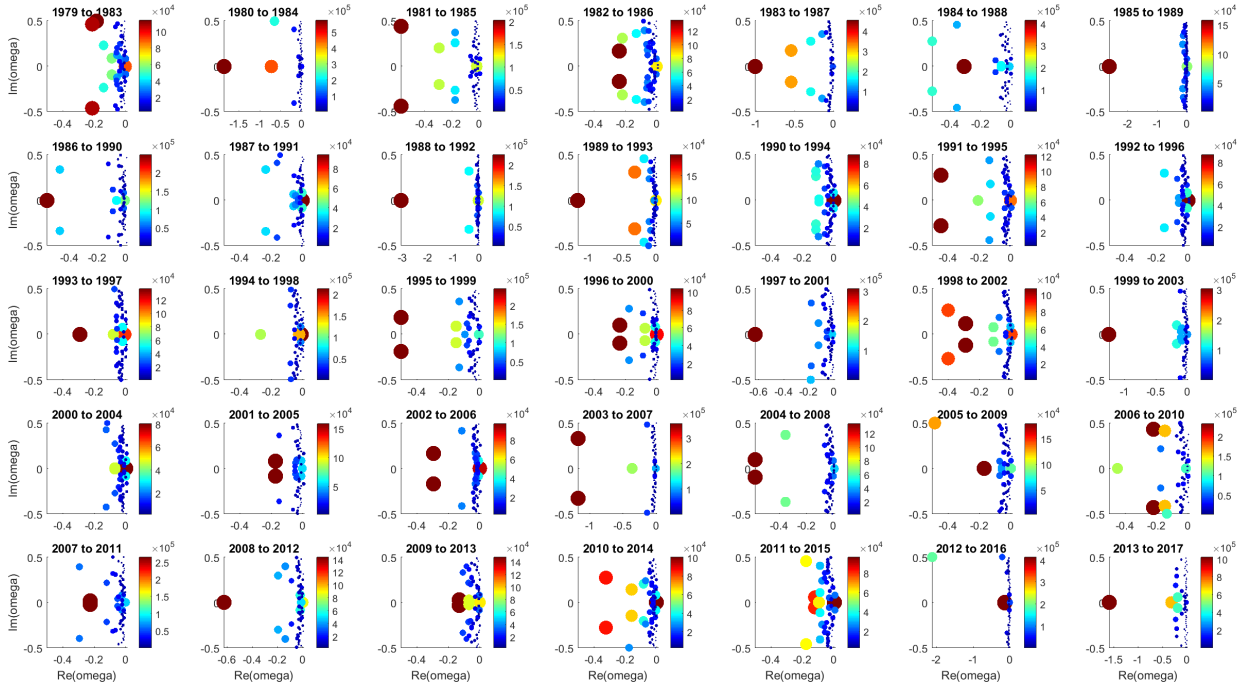


Figure 5: Southern hemisphere Koopman eigenvalues for 5 year time windows beginning in 1979. Each circle corresponds to the eigenvalue of a Koopman mode, where the size and color of the circle are both representations of the L2 norm of the corresponding mode, the position along the horizontal axis shows the growth or decay constant of the mode (e.g. the more negative the value the faster the mode decays), and the position along the vertical axis shows the oscillatory frequency of the mode. The time scale is in months, so the two circles generally visible at approximately $\pm 0.08$ on the vertical axis are the expected annual variation of the sea ice concentration. As in the northern hemisphere case, the novel result apparent is the mostly consistent presence of a large norm mode near the origin beginning in the 1990's.

dependence. These modes show that the decrease in sea ice concentration is most pronounced in the regions of the Beaufort Sea and the Arctic Ocean north of European Russia, consistent with the changes in the mean and annual variation oberved in the five year window cases above.

### Comparison of Koopman Eigenvalues and Modes for Sea Ice Concentration and Thickness

To compare the dynamical behavior of the sea ice concentration and thickness over the time period considered, we compared the Koopman eigenvalues for both data sets and the geographical distribution of the Koopman modes corresponding to the mean and annual variation. Figure 11 shows the eigenvalues for the two data sets over the same five year window (2013-2017). Their eigenvalue distributions are similar, which is consistent with the expectation that the observables in each case will have similar time dependence.

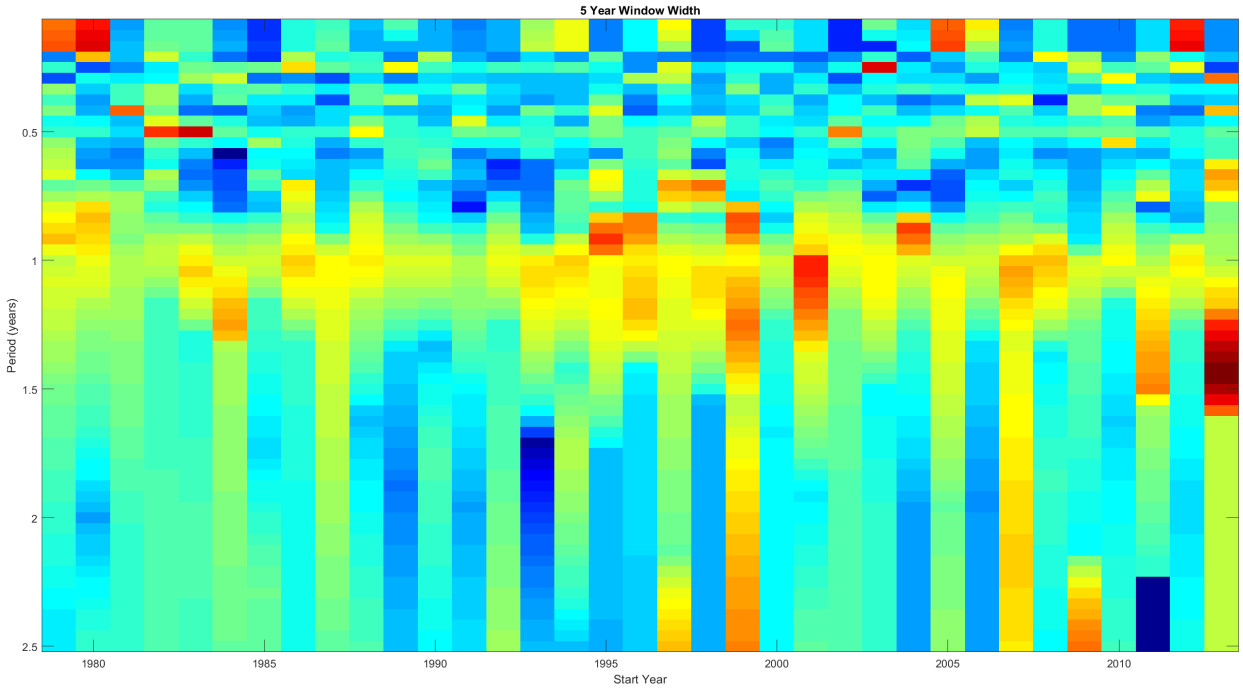


Figure 6: Southern hemisphere Koopman spectrogram showing period (in years) of eigenvalues. The consistent peak at one year represents the annual variation in sea ice concentration.

Before examining the Koopman modes, we examined the maximum values each pixel in the two data sets obtained over the five year range considered here. The concentration and thickness data sets were measured using different instruments on different satellites and therefore do not have identical geographic coverage. A second important difference between the observables is that the concentration data values are necessarily bounded, as by its definition concentration cannot be less than zero or greater than 100% (represented here by a value of 1000), wheres the thickness data is measured in meters and can thus in principle have any value greater than or equal to zero. Figure 12 shows that while the thickness data was measured over a more limited geographic region than the concentration data, the unbounded nature of the thickness data reveals greater structure within ice-filled regions than the concentration data can show.

We now examine the geographic significance of the Koopman modes corresponding to the mean and annual variation over the five year time window. Figure 13 shows that, within their overlapping regions of coverage, the two data sets show similar results. The mean modes have their greatest values to the north of Greenland, and significant annual variation is seen north of Alaska and eastern Siberia. The effect of the greater local structure present in the thickness data is seen by the smaller scale details of the annual variation visible in the thickness mode as compared to the concentration mode. The concentration annual variation is largest in the regions between the minimum and maximum extent of the sea ice, whereas the thickness mode also shows the variation of the thickness of the sea ice in regions that remain ice covered for all or most of the year, e.g. north of Svalbard.

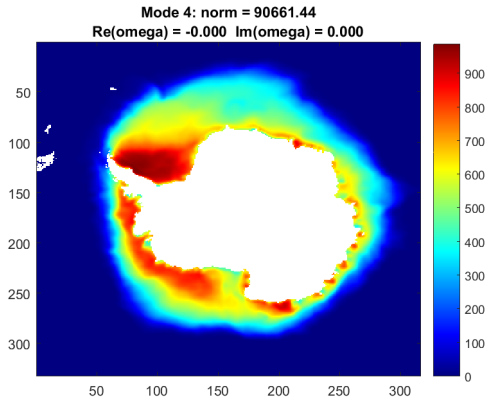


(a) Mean mode, 1979-1983.

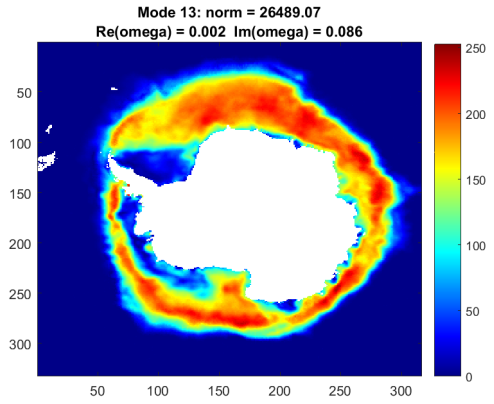


(b) Annual variation mode, 1979-1983.

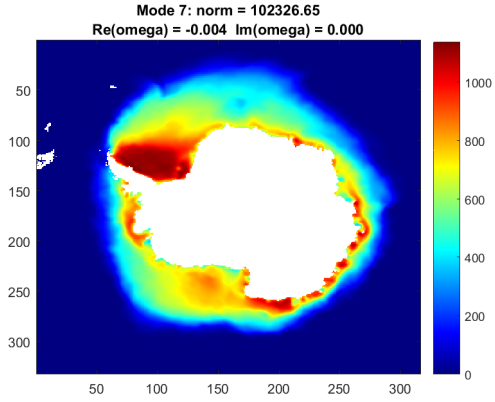


(c) Mean mode, 2013-2017.

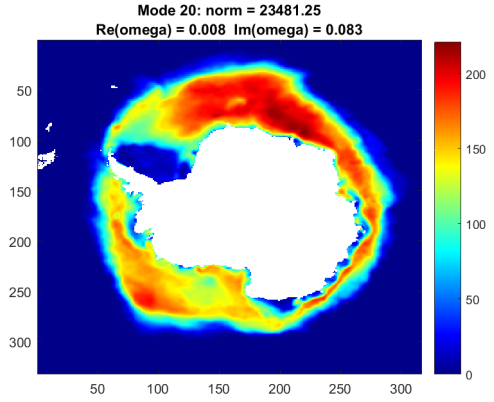


(d) Annual variation mode, 2013-2017.

Figure 7: Koopman modes representing the mean and annual variation in sea ice concentration over five year windows for the southern hemisphere. (a) Mean concentration, 1979-1983 period, (b) annual variation, 1979-1983 period, (c) mean concentration, 2013-2017 period, (d) annual variation, 2013-2017 period. A general decrease in sea ice concentration is apparent, particularly near West Antarctica.

### Prediction of Future Sea Ice Concentration

Figures 14 to 21 show example northern hemisphere sea ice concentration prediction results compared with the actual sea ice concentration for the same month. The data shown are the predictions for January and July for the four years following the five year window 1979-1983 that was used as the input data for KMD. It is seen that the prediction results match the general extent and magnitude of the actual data as well as capturing many small scale features such as the shape of the concentration near the east coast of Greenland. The predictions are also seen to be less accurate in later months, particularly in specific details such as the concentration in the Sea of Okhotsk.

Figures 22 to 29 show example southern hemisphere sea ice concentration prediction results compared with the actual sea ice concentration for the same month. The data shown are the predictions for January and July for the four years following the five year window

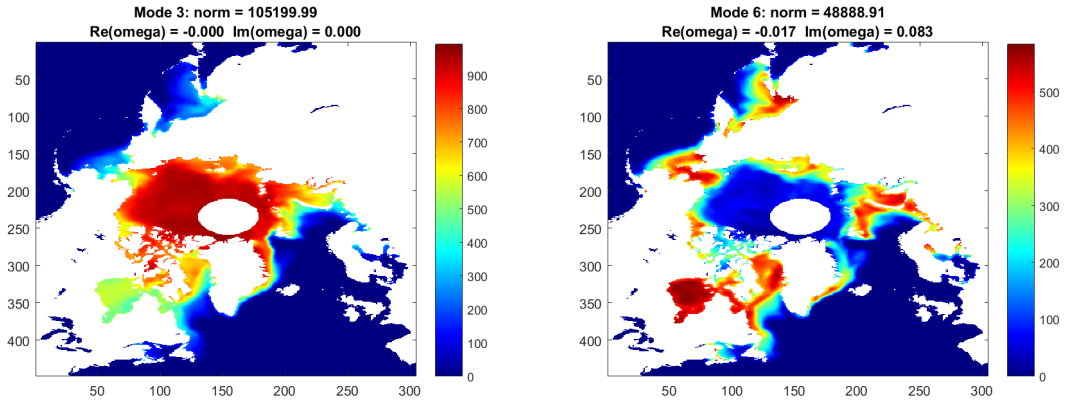


(a) Mean mode, 1979-1983.

(b) Annual variation mode, 1979-1983.

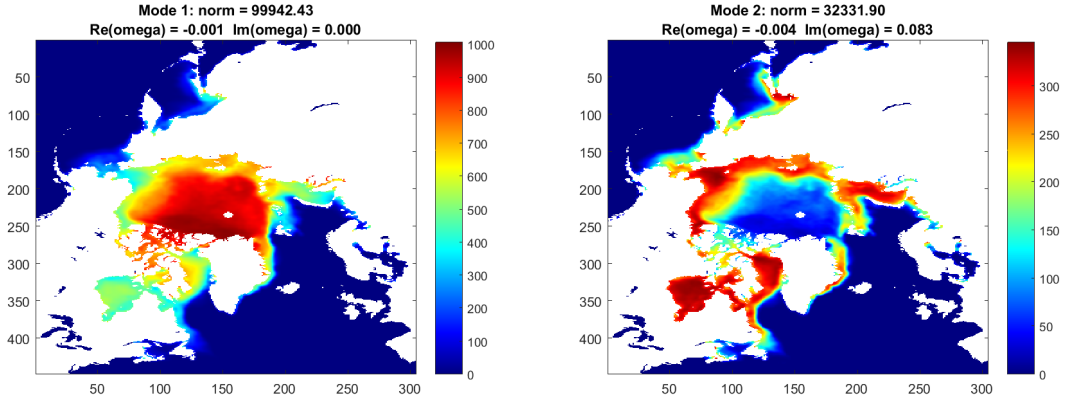


(c) Mean mode, 2013-2017.

(d) Annual variation mode, 2013-2017.

Figure 8: Koopman modes representing the mean and annual variation in sea ice concentration over five year windows for the northern hemisphere. (a) Mean concentration, 1979-1983 period, (b) annual variation, 1979-1983 period, (c) mean concentration, 2013-2017 period, (d) annual variation, 2013-2017 period. A general decrease in sea ice concentration is apparent, particularly in the Beaufort and Kara seas.

1979-1983 that was used as the input data for KMD. Again, it is seen that the prediction results match the general extent and magnitude of the actual data as well as capturing many small scale features.

Figure 30 shows the actual mean sea ice concentrations for the 39 year period of data for the northern hemisphere regions considered here. The breakdown of the sea ice concentration into different regions shows the geographic variation in dynamics. Some regions, such as the Hudson Strait, Hudson Bay, and Chukchi Sea, consistently vary between nearly 100% sea ice concentration in the winter and 0% coverage in the summer, while most other regions show greater year-to-year variation in maximum or minimum sea ice concentration. The regions in this latter case are of greatest interest for prediction techniques, as it is desirable to, for example, correctly predict the future behavior of the summer sea ice concentration in the Arctic Ocean (see the subplot in the center of the bottom row in Figure 30) .

Figure 31 shows the actual mean sea ice concentrations for the 39 year period of data for

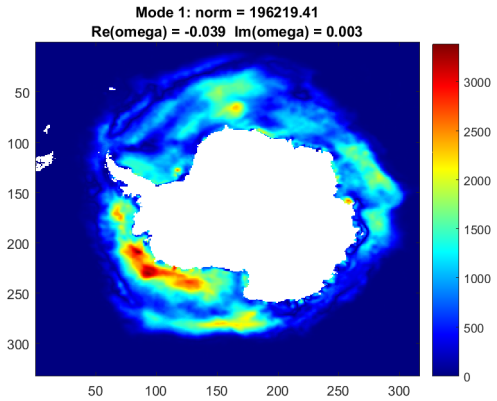


Figure 9: Mode from entire 39 year data set showing long term decrease in sea ice off West Antarctica.

the southern hemisphere regions. The character of the southern hemisphere differs from the northern hemisphere, as expected due to the large scale geographical differences. The Indian Ocean and West Pacific Ocean show relatively consistent seasonal variations, and the Ross Sea behaves somewhat like an Arctic sea with its large consistent seasonal variations, but the Weddell, Amundsen, and Bellingshausen Seas show a large degree of year-to-year variability in mean sea ice concentration. Also note that while the Amundsen and Bellingshausen Seas show temporal variation of a similar character, their multi-year variations are not obviously correlated, which motivated our decision to consider them are separate regions.

Figure 32 shows the results for the first method of judging the goodness of the prediction (the mean of the absolute difference between the actual and predicted results), for the northern hemisphere for predictions for 2014-2017 using the previous 30 years of data. This plot shows, in effect, the expected error of the prediction for a given pixel in each region. Seasonal variation is apparent, but interestingly the error does not always increase year to year. The error is also generally largest in the seas around the Arctic Ocean (the Kara, Laptev, East Siberian, Chukchi, etc.) where the seasonal variation in sea ice concentration is most pronounced.

Figure 33 shows a different view of the goodness of the northern hemisphere prediction, showing the mean of the actual data (blue lines) and predictions (red lines) for each region. This shows the general trends of sea ice concentration in each region, rather than being a pixel-to-pixel comparison of the actual and predicted results. Here we see that the various Arctic seas mentioned above and other regions with large seasonal variations show good agreement between the actual and predicted results. This implies that while the prediction may not always be geographically precise in predicting the distribution of sea ice concentration within a particular region, it is generally successful at predicting the average sea ice concentration within the region. Close examination of regions of interest, particularly the Arctic Ocean, shows that the prediction does not always closely match the summer minimum in sea ice concentration, but in this case the prediction does match the trend of the actual result (i.e., the summer minimum decreases year to year for the first three years, then it increases in the fourth year).

The goodness measures of the prediction for the southern hemisphere regions are shown in

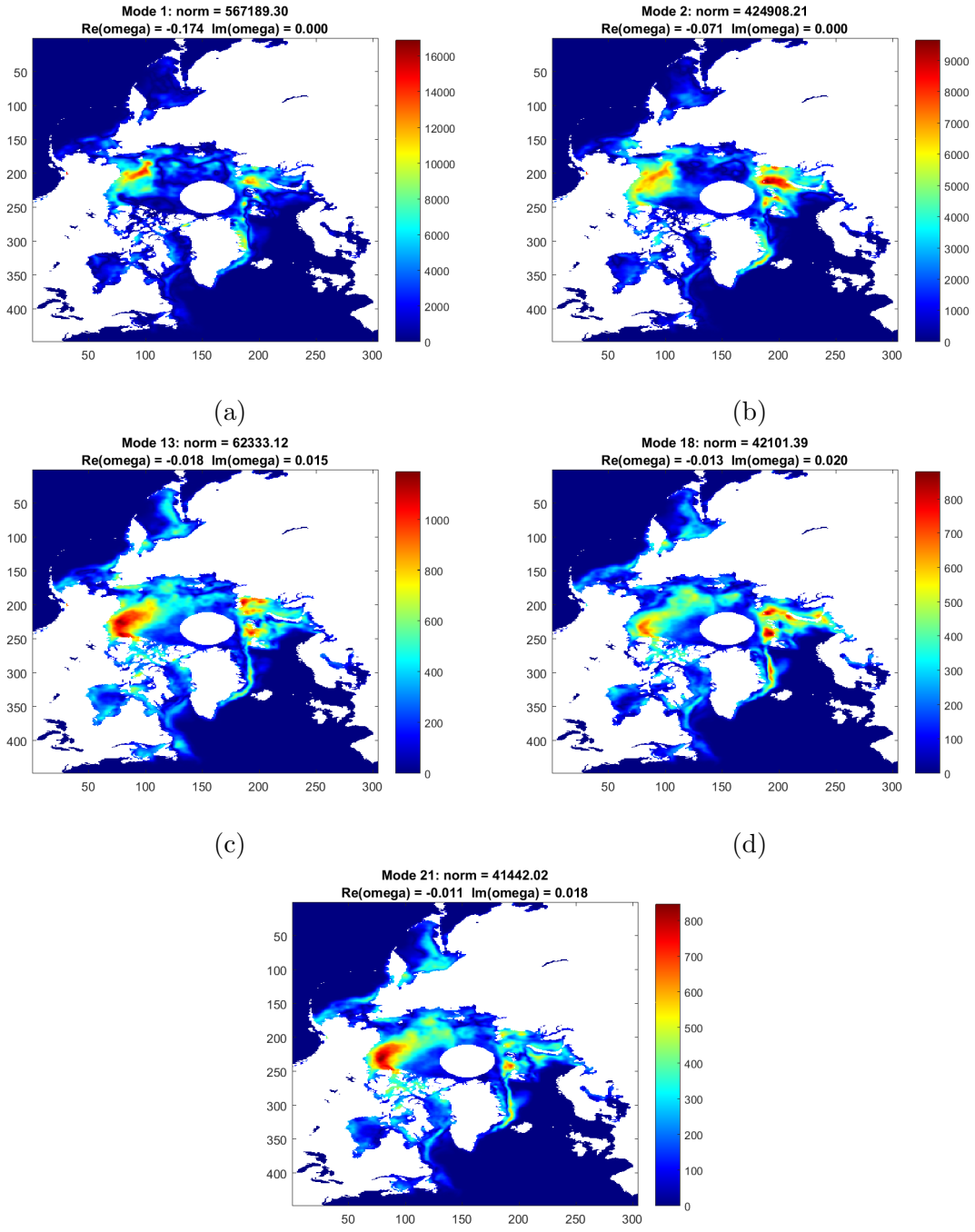


Figure 10: Modes from entire 39 year data set for the northern hemisphere, showing long term decrease in sea ice north of Alaska and European Russia.

Figures 34 and 35. Figure 34 shows the results for the first method of judging the goodness of the prediction (the mean of the absolute difference between the actual and predicted results), for the southern hemisphere for predictions for 2014-2017 using the previous 30 years of data.

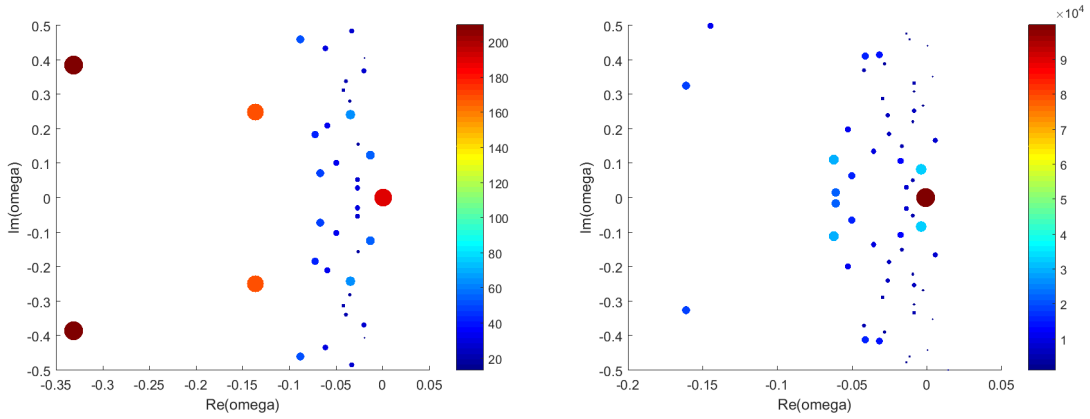


(a) Thickness eigenvalues. (b) Concentration eigenvalues.

Figure 11: Comparison of Koopman eigenvalues for sea ice thickness and concentration over a five year window of 2013 to 2017 for the northern hemisphere. (a) Thickness eigenvalues, (b) concentration eigenvalues. Both cases show conjugate pairs of modes corresponding to annual variation (at $\pm 0.125$ on the vertical axis for the thickness data and at $\pm 0.083$ for the concentration data) and biannual variation (at $\pm 0.250$ and $\pm 0.167$ on the vertical axes for thickness and concentration data, respectively) as well as a generally similar distribution of other modes.

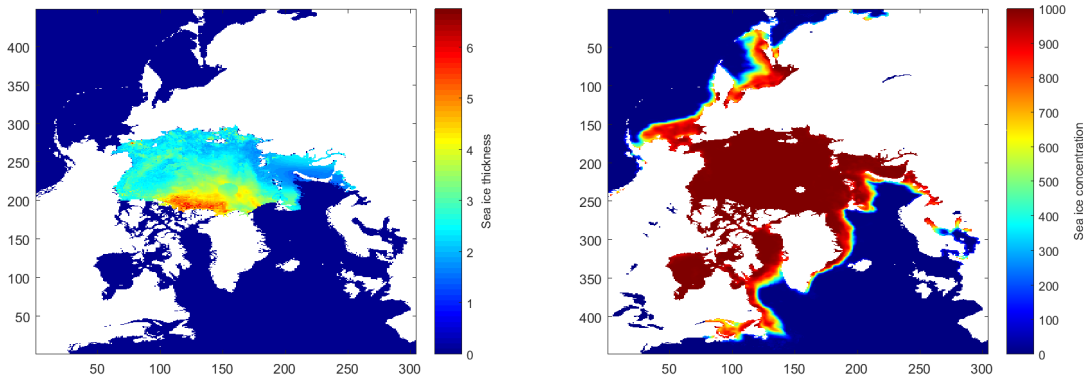


(a) Maximum thickness (meters) (b) Maximum concentration (1000 = 100%)

Figure 12: Maximum values obtained for each pixel in the thickness and concentration data sets. The thickness data is only available over a restricted region in and around the Arctic Ocean, while the concentration data is available over a wider region. The thickness data is also seen to have more structure visible because the maximum thickness values are not bounded, whereas concentration cannot exceed 100% (a pixel value of 1000).

The error is similar for each region, and shows an apparent slow increase over time.

Figure 35 shows the mean of the actual data (blue lines) and predictions (red lines) for each region, showing the general trends of sea ice concentration in each region. It is seen that in the first year, the prediction of the maximum sea ice concentration is very good for

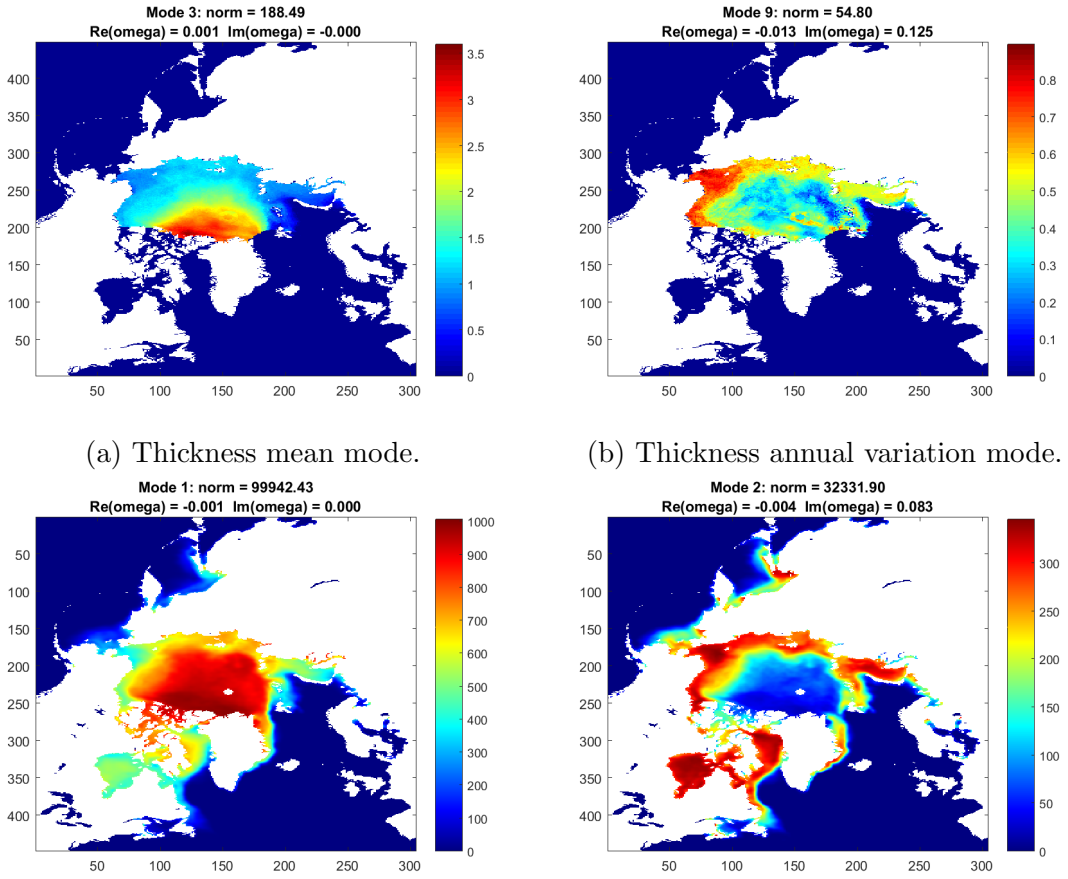


(a) Thickness mean mode.

(b) Thickness annual variation mode.

(c) Concentration mean mode.

(d) Concentration annual variation mode.

Figure 13: Comparison of Koopman modes representing the mean and annual variation in sea ice thickness and concentration over a five year window of 2013 to 2017 for the northern hemisphere. (a) Mean thickness, (b) thickness annual variation, (c) mean concentration, (d) concentration annual variation. The same geographic patterns are apparent in the mean and annual variations, in that the mean thickness and concentration are largest to the north of Greenland, and the annual variation is largest north of Alaska and eastern Siberia. An interesting difference in the annual variation modes is the presence of localized spots of annually varying thickness north of Svalbard.

each region, and even the minimum for the following year is well predicted in the Weddell Sea, West Pacific, and Amundsen Sea.

Figures 36 to 43 are 2-D representations of the goodness of the prediction for the next year, for the single months of the year with the minimum and maximum sea ice extent for varied KMD window widths. The goodness measure is the error of the prediction result, specifically the difference between the prediction result and the actual sea ice concentration for a particular month (recall that here concentration is shown in tenths of a percent, i.e. 1000 corresponds to 100% concentration). The horizontal axis of the figure is the year of the month predicted, and the vertical axis is the number of years used as the input to the Koopman mode decomposition used to perform future prediction. Note that for each

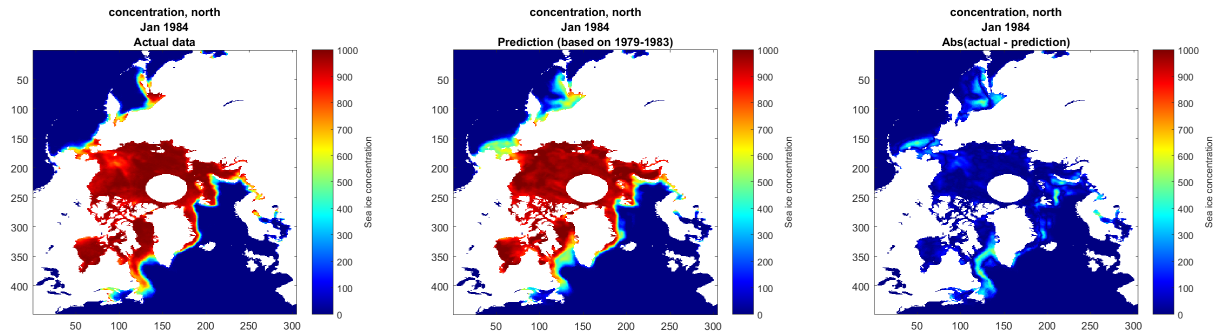


Figure 14: January 1984, 1 month after 1979-1983 input data. Left: actual concentration. Middle: predicted concentration. Right: Absolute difference between actual and predicted concentration

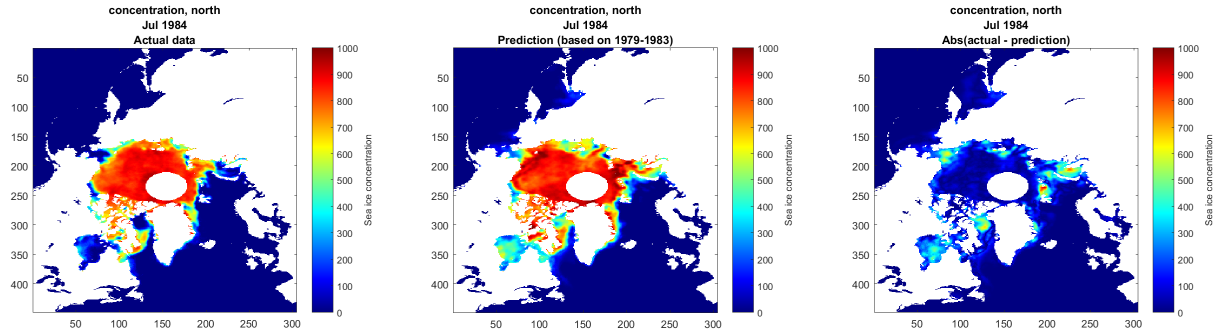


Figure 15: July 1984, 7 months after 1979-1983 input data. Left: actual concentration. Middle: predicted concentration. Right: Absolute difference between actual and predicted concentration

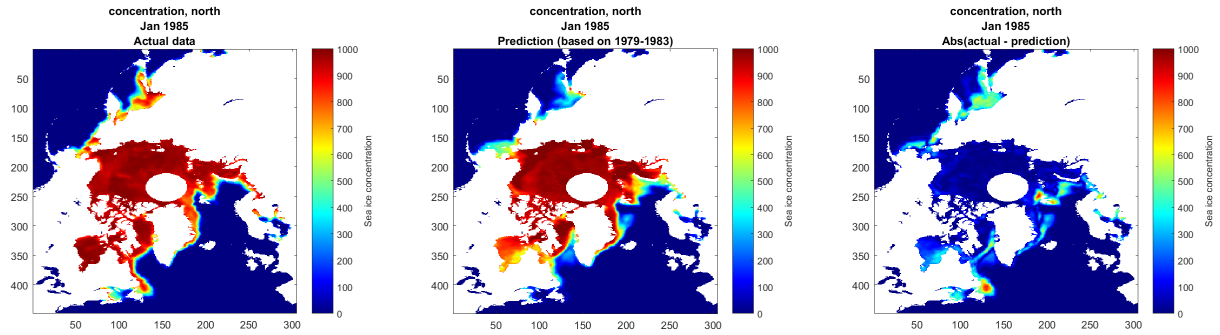


Figure 16: January 1985, 13 months after 1979-1983 input data. Left: actual concentration. Middle: predicted concentration. Right: Absolute difference between actual and predicted concentration

prediction year, the year range used for KMD prediction immediately precedes the prediction year, e.g. for prediction year 2017, a 3 year window width consists of the years 2014-2016,

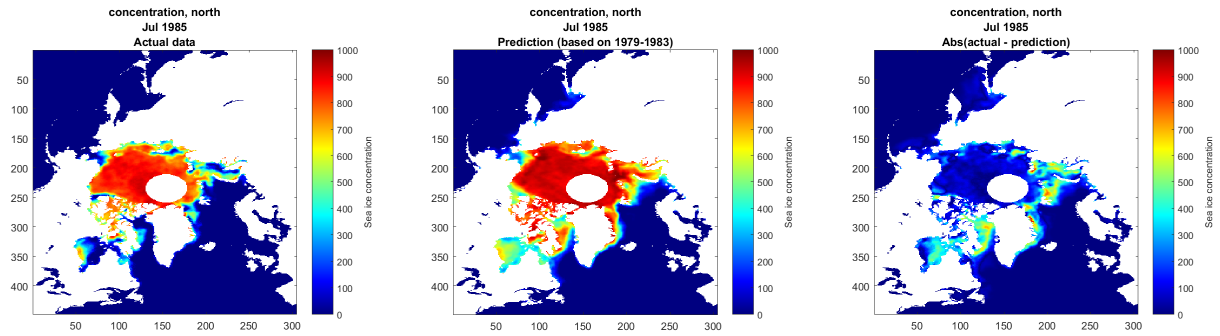


Figure 17: July 1985, 19 months after 1979-1983 input data. Left: actual concentration. Middle: predicted concentration. Right: Absolute difference between actual and predicted concentration

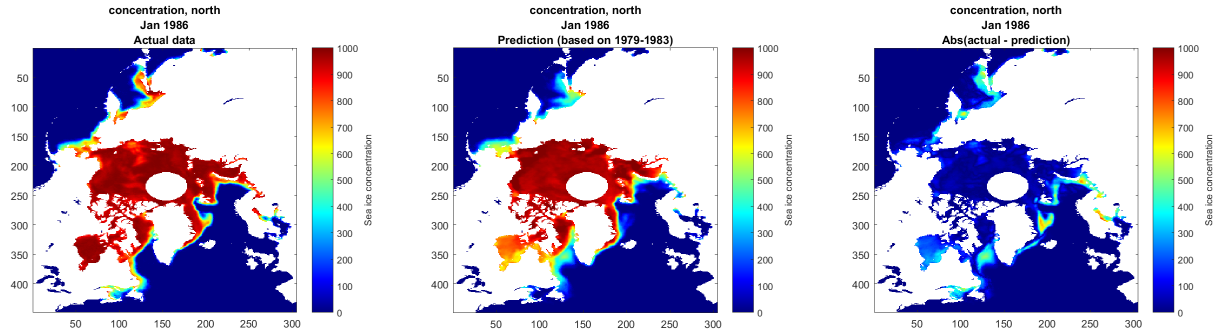


Figure 18: January 1986, 25 months after 1979-1983 input data. Left: actual concentration. Middle: predicted concentration. Right: Absolute difference between actual and predicted concentration

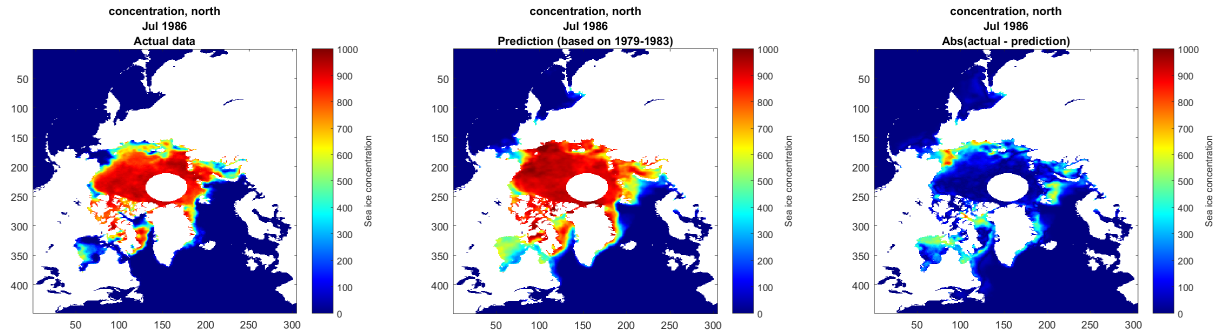


Figure 19: July 1986, 31 months after 1979-1983 input data. Left: actual concentration. Middle: predicted concentration. Right: Absolute difference between actual and predicted concentration

a 10 year window width consists of the years 2007-2016, and so on. Because the sea ice concentration data used is only available starting from the year 1979, the maximum possible

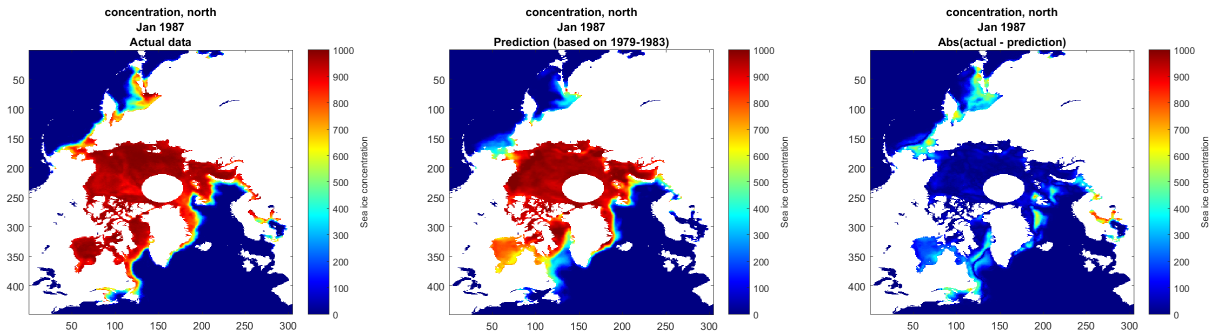


Figure 20: January 1987, 37 months after 1979-1983 input data. Left: actual concentration. Middle: predicted concentration. Right: Absolute difference between actual and predicted concentration

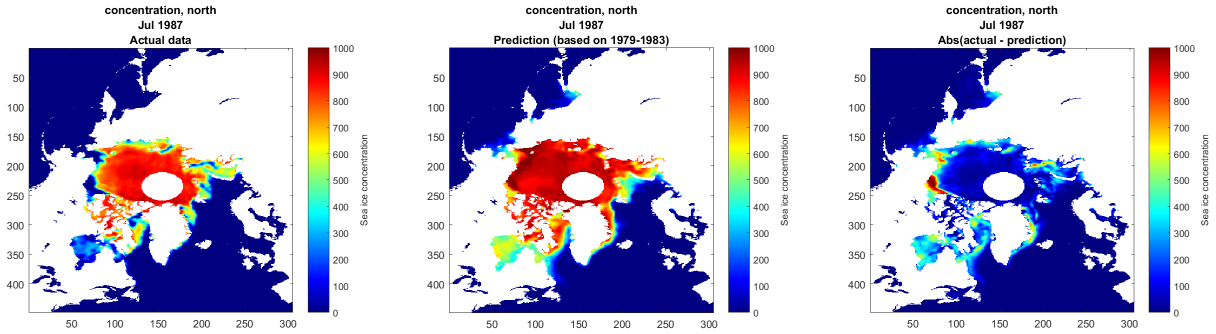


Figure 21: July 1987, 43 months after 1979-1983 input data. Left: actual concentration. Middle: predicted concentration. Right: Absolute difference between actual and predicted concentration

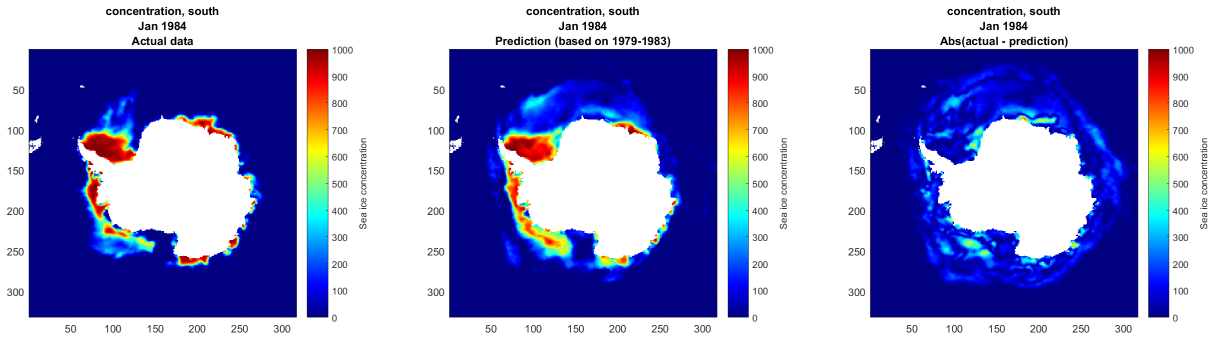


Figure 22: January 1984, 1 month after 1979-1983 input data. Left: actual concentration. Middle: predicted concentration. Right: Absolute difference between actual and predicted concentration

window width increases by one year per year after 1979, up to a maximum window width of 38 years for predictions of the year 2017. The minimum window width was chosen to

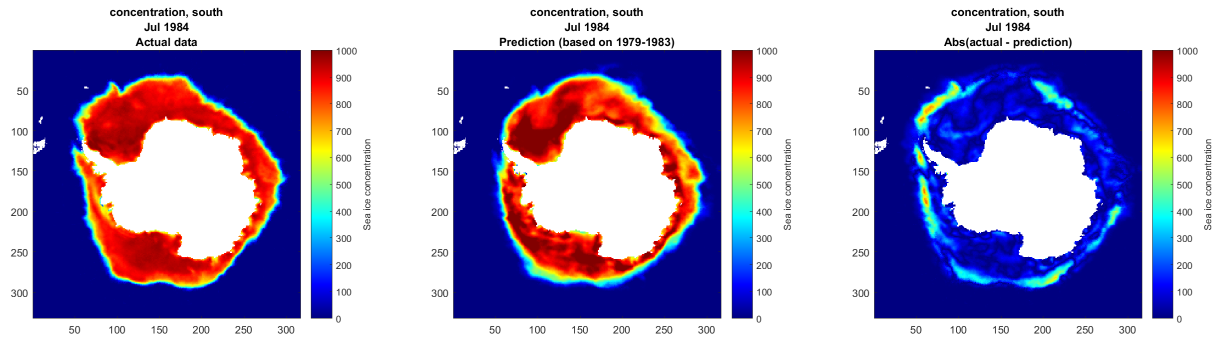


Figure 23: July 1984, 7 months after 1979-1983 input data. Left: actual concentration. Middle: predicted concentration. Right: Absolute difference between actual and predicted concentration

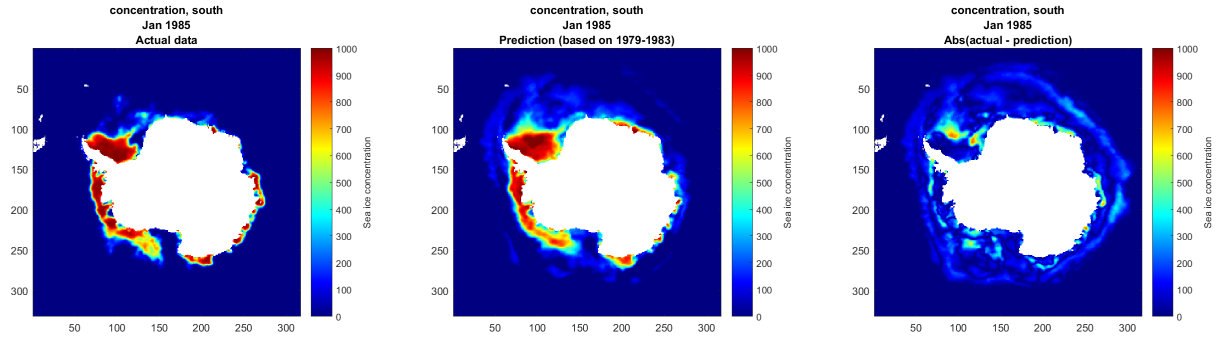


Figure 24: January 1985, 13 months after 1979-1983 input data. Left: actual concentration. Middle: predicted concentration. Right: Absolute difference between actual and predicted concentration

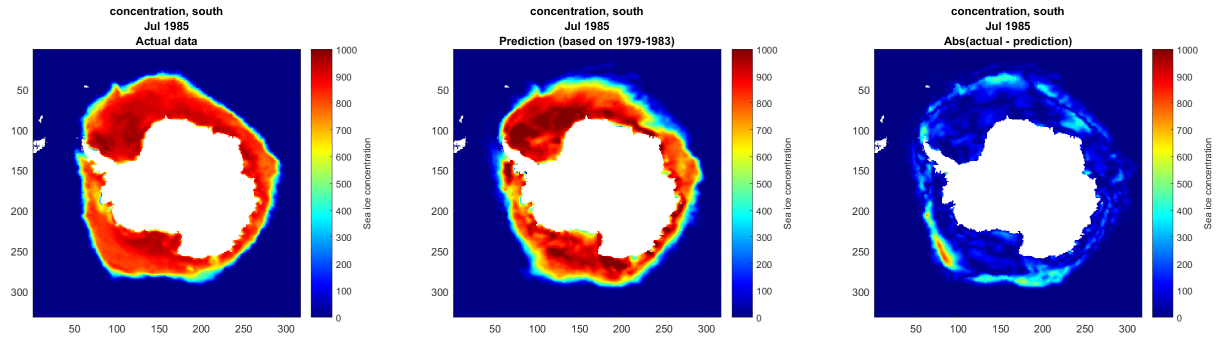


Figure 25: July 1985, 19 months after 1979-1983 input data. Left: actual concentration. Middle: predicted concentration. Right: Absolute difference between actual and predicted concentration

be 3 years, so the figures show prediction years between 1982 and 2017 and window widths between 3 and 38 years.

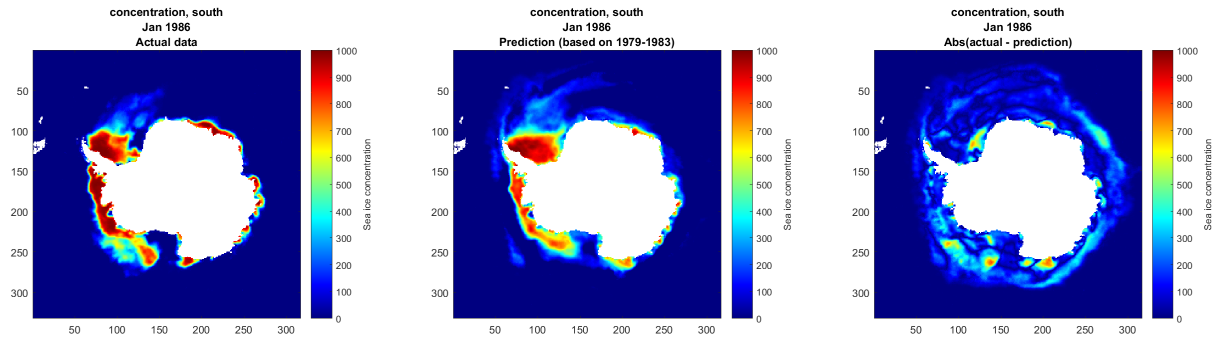


Figure 26: January 1986, 25 months after 1979-1983 input data. Left: actual concentration. Middle: predicted concentration. Right: Absolute difference between actual and predicted concentration

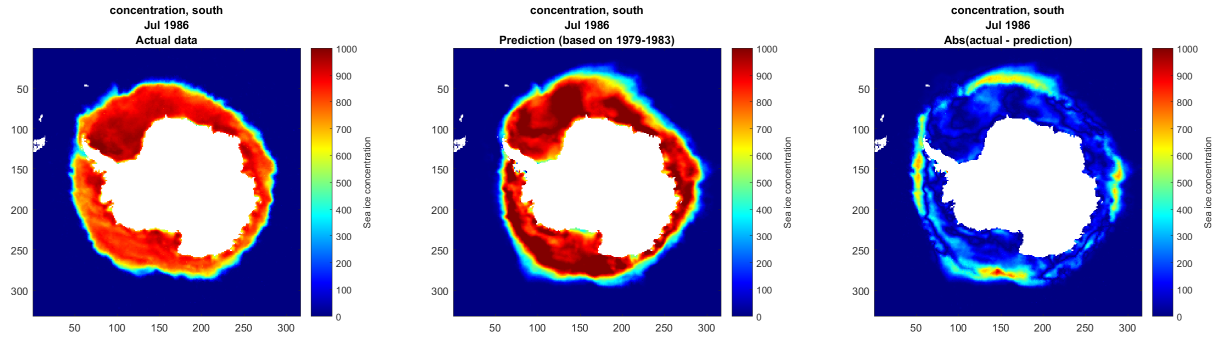


Figure 27: July 1986, 31 months after 1979-1983 input data. Left: actual concentration. Middle: predicted concentration. Right: Absolute difference between actual and predicted concentration

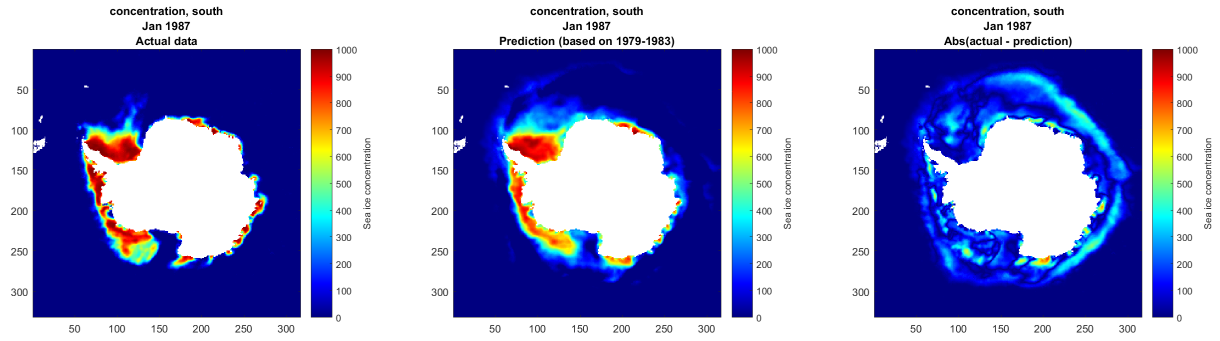


Figure 28: January 1987, 37 months after 1979-1983 input data. Left: actual concentration. Middle: predicted concentration. Right: Absolute difference between actual and predicted concentration

The color scale of the figures highlights the deviation from zero of the prediction error, where red and blue show when the prediction is greater than or less than the actual data,

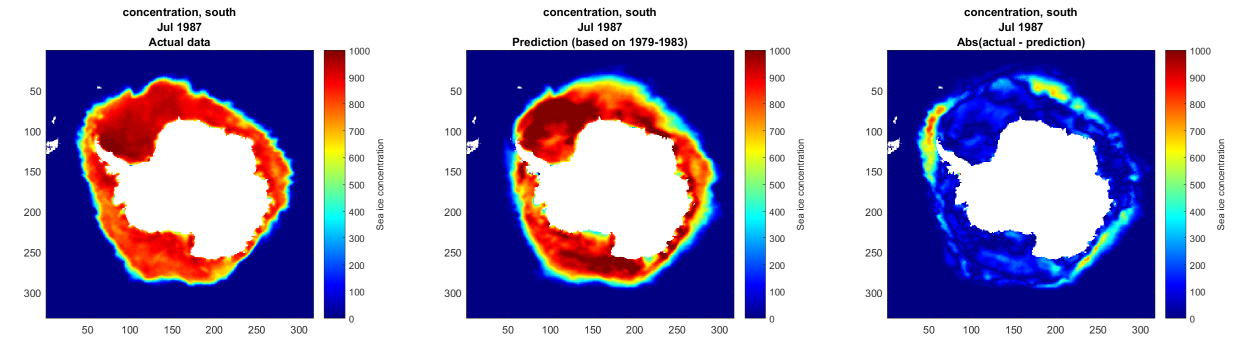


Figure 29: July 1987, 43 months after 1979-1983 input data. Left: actual concentration. Middle: predicted concentration. Right: Absolute difference between actual and predicted concentration

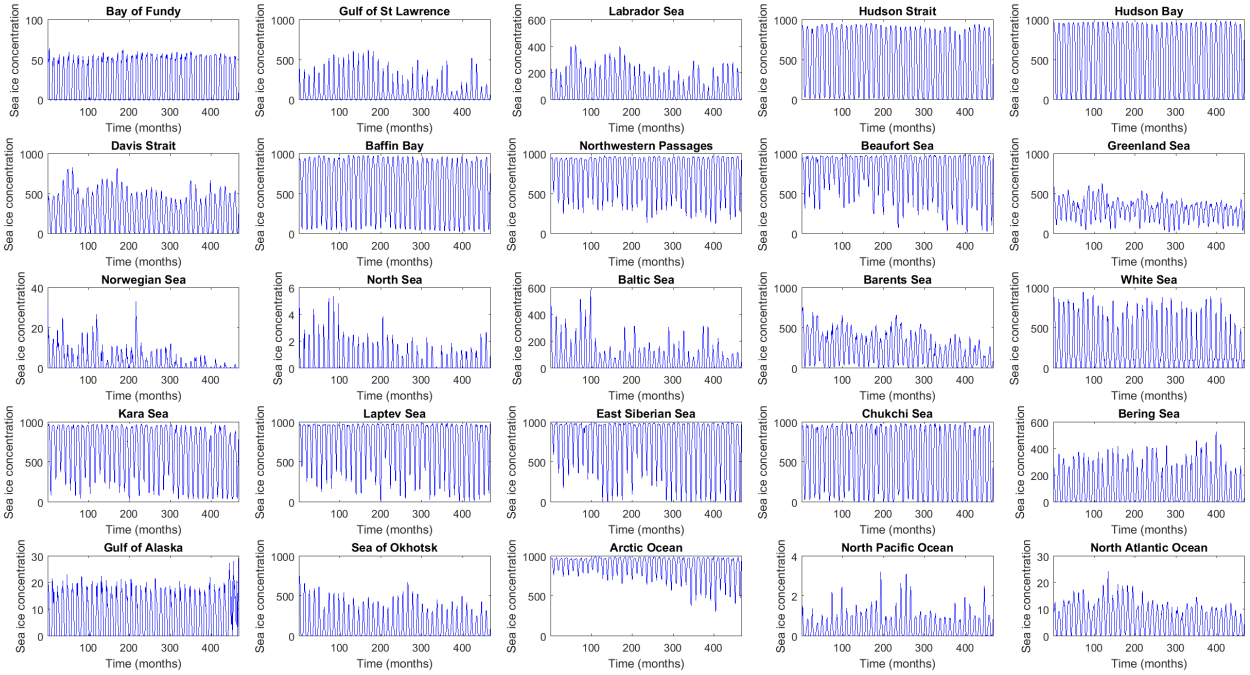


Figure 30: Time series of monthly average sea ice concentration (1000=100%) for northern hemisphere regions.

respectively, and darker colors indicate larger magnitude errors (note that the color maps are not symmetric about zero, however). Points that are colored white indicate that the prediction was in good agreement with the actual data, therefore regions of white or light colors indicate combinations of window widths and prediction years that were found to successfully predict future sea ice annual minimum and maximum concentrations. Large regions of white/light colors are of more interest than isolated pixels, because robust prediction capabilities are desired, and isolated prediction successes could be attributed to random chance rather than legitimate predictive ability.

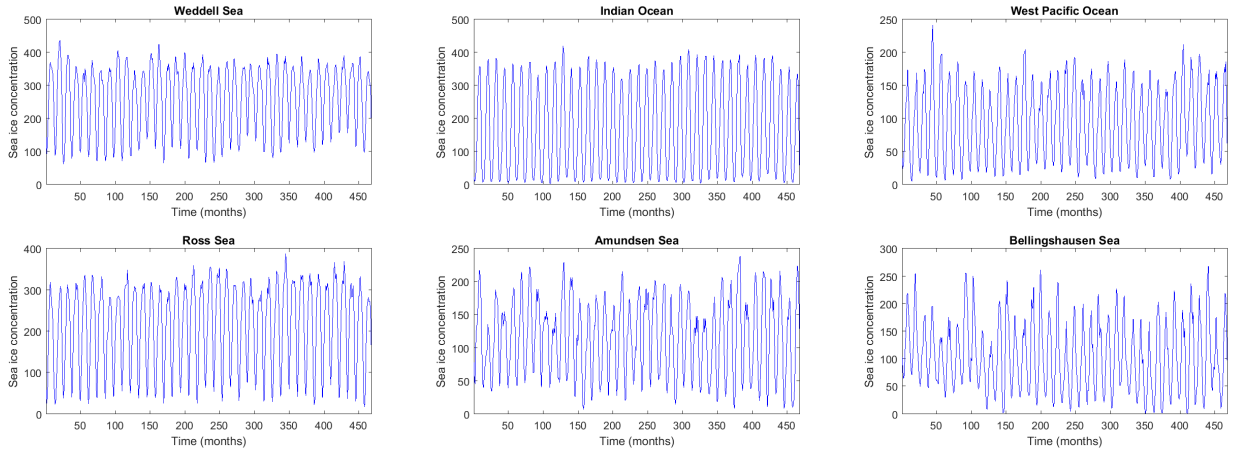


Figure 31: Time series of monthly average sea ice concentration (1000=100%) for southern hemisphere regions.

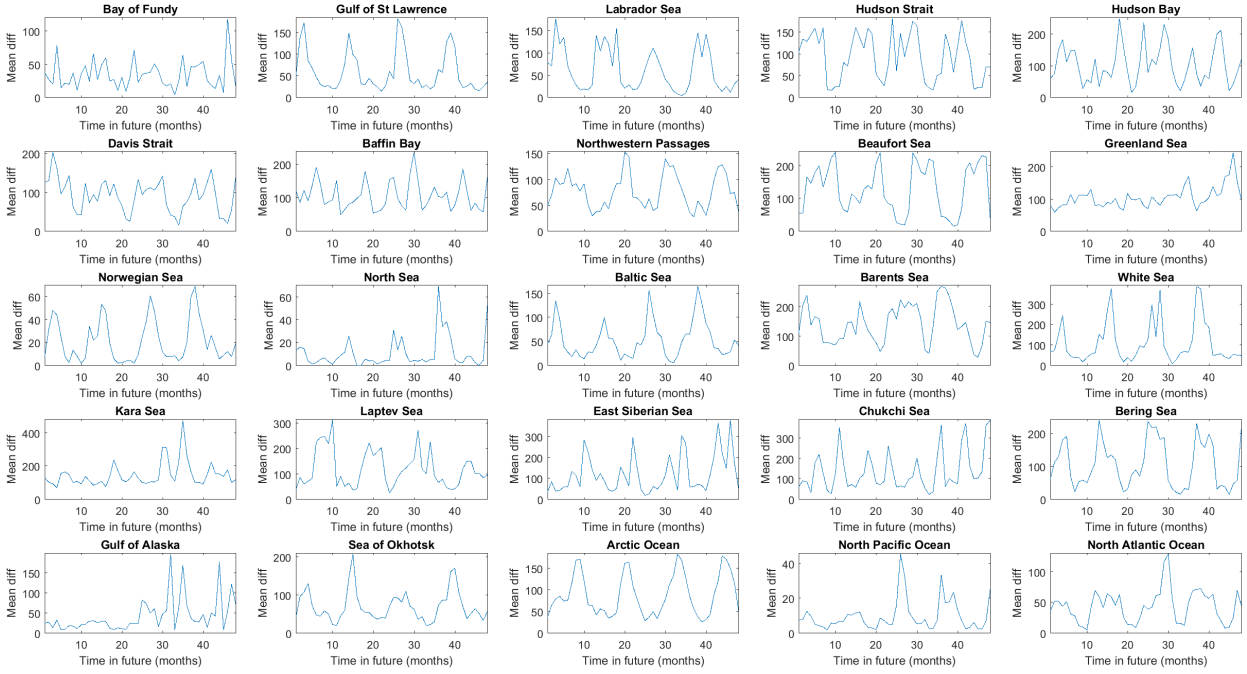


Figure 32: Goodness of northern hemisphere prediction results, based on summing the absolute value of the difference between the actual data and prediction results for all pixel values for which either the actual data or prediction results contained a sea ice concentration value greater than zero. Prediction is based on KMD of 30 year data range (1984 to 2013) and prediction of four future years. Vertical axis units are sea ice concentration (1000=100%).

Figure 36 shows the prediction error for March (when the sea ice annual concentration maximum occurs) for the entire region of the northern hemisphere covered by the available satellite data. For most years, the best prediction results occur for windows of at least 10

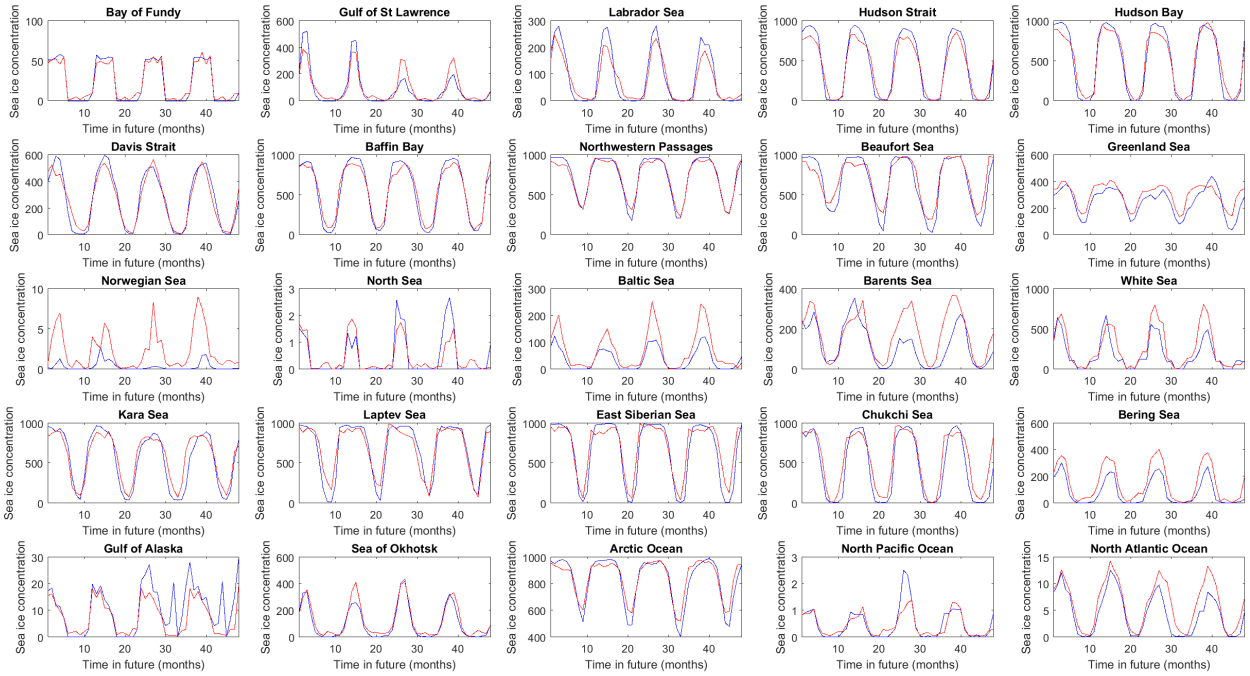


Figure 33: Comparison of actual (blue) and predicted (red) northern hemisphere mean sea ice concentration. Prediction is based on KMD of 30 year data range (1984 to 2013) and prediction of four future years. Vertical axis units are sea ice concentration (1000=100%).

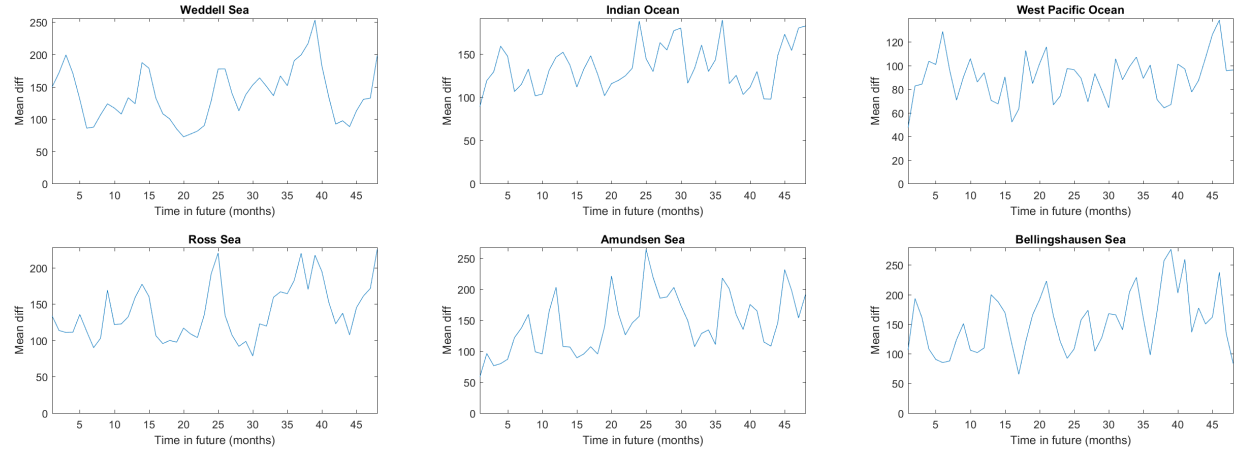


Figure 34: Goodness of southern hemisphere prediction results, based on summing the absolute value of the difference between the actual data and prediction results for all pixel values for which either the actual data or prediction results contained a sea ice concentration value greater than zero. Prediction is based on KMD of 30 year data range (1984 to 2013) and prediction of four future years. Vertical axis units are sea ice concentration (1000=100%).

years and the goodness generally improves with window width. Years where the prediction goodness is relatively poor and does not significantly improve with increasing window width

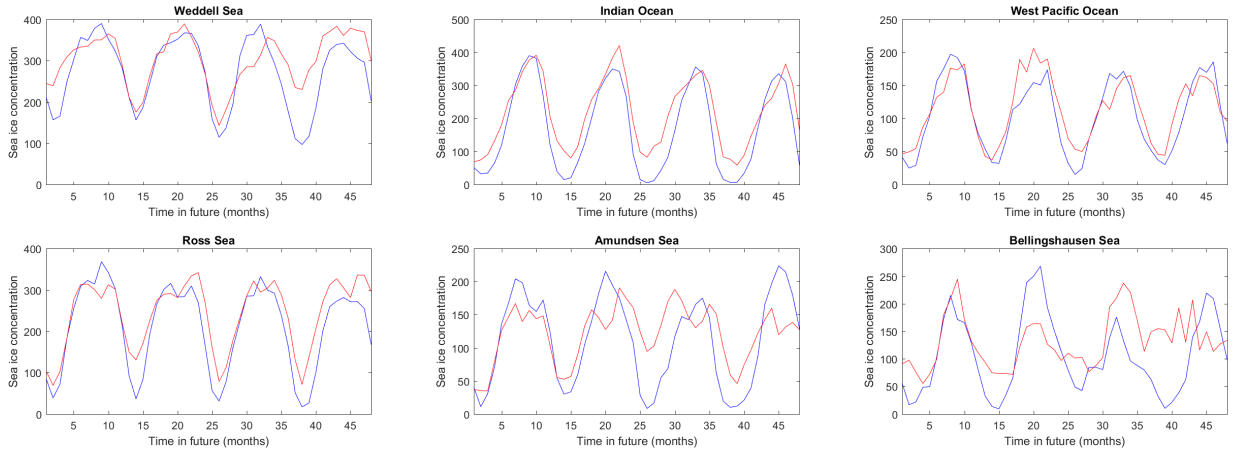


Figure 35: Comparison of actual (blue) and predicted (red) southern hemisphere mean sea ice concentration. Prediction is based on KMD of 30 year data range (1984 to 2013) and prediction of four future years. Vertical axis units are sea ice concentration (1000=100%).

are generally years with a large change from one year to the next.

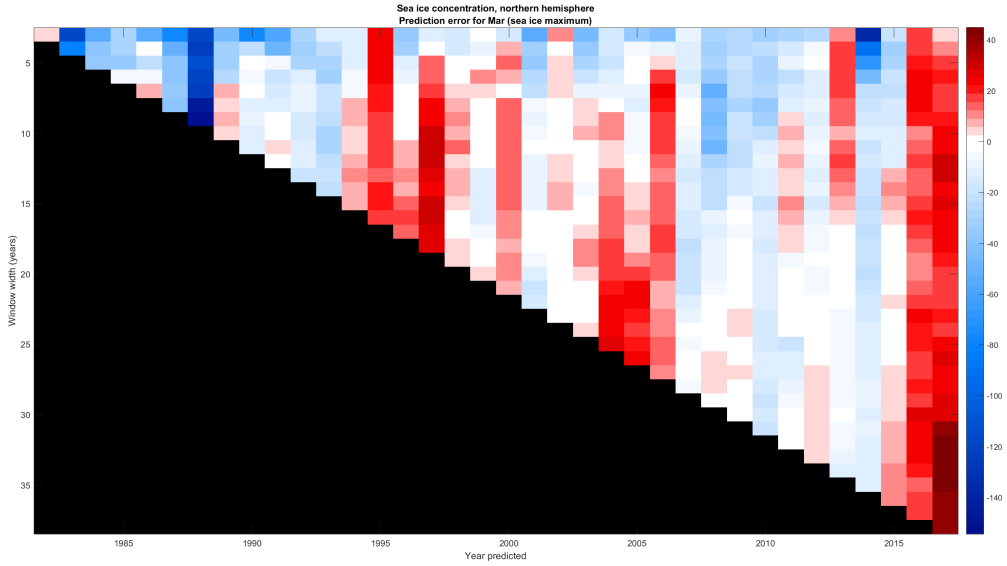


Figure 36: Sea ice concentration prediction error for the entire northern hemisphere region covered by the available satellite data, for the month of March, when the maximum sea ice concentration occurs. The best prediction results generally occur for longer time windows.

Figure 37 shows the prediction error for September for the entire covered region of the northern hemisphere, when the sea ice annual minimum occurs. In contrast to the results for the sea ice maximum, the prediction error is not generally better for longer windows.

Figures 38 and 39 show northern hemisphere prediction results for March and September for specific geographic regions. Generally, longer windows are seen to produce better prediction results, but there is significant variation between different regions and no single

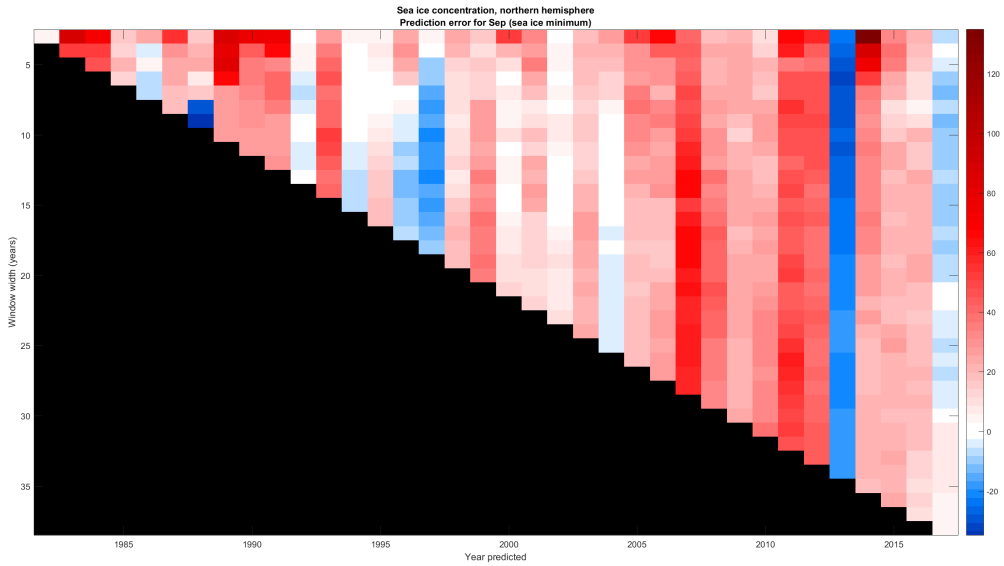


Figure 37: Sea ice concentration prediction error for the entire northern hemisphere region covered by the available satellite data, for the month of September, when the minimum sea ice concentration occurs. Here, longer windows do not as often produce better prediction results.

window width range is obviously best for all cases. This difference is presumably due to the different time scales and degree of influence of the different effects driving the dynamics of different regions.

Figures 40 to 43 show the equivalent set of figures for the southern hemisphere, where September is the month with the maximum sea ice concentration and February (not March) is the month with the minimum sea ice concentration. The same general comments apply to the southern hemisphere results as to northern hemisphere results, with the important difference that longer windows are generally of less benefit in the southern hemisphere case.

## Conclusions

General conclusions from the application of Koopman Mode decomposition and analysis techniques to sea ice data is that these techniques can reveal meaningful insights into the temporal and spatial dynamics of sea ice behavior.

Specifically, the results showed the consistency of the Koopman analysis technique as applied to sea ice concentration data from the northern and southern hemispheres, as well as the ability of the analysis to identify geographic regions undergoing long-term decreases in sea ice concentration. The results for the sea ice concentration and thickness data sets shows the expected consistency in their dynamical behavior and also additional localized variations present in the thickness data that the bounded concentration data does not show. For prediction, KMD was found to produce relatively accurate predictions over several years of future sea ice concentration values for a range of multiyear data windows and was found to work well for some regions, as Arctic seas, and produce useful predictions for the Arctic Ocean.

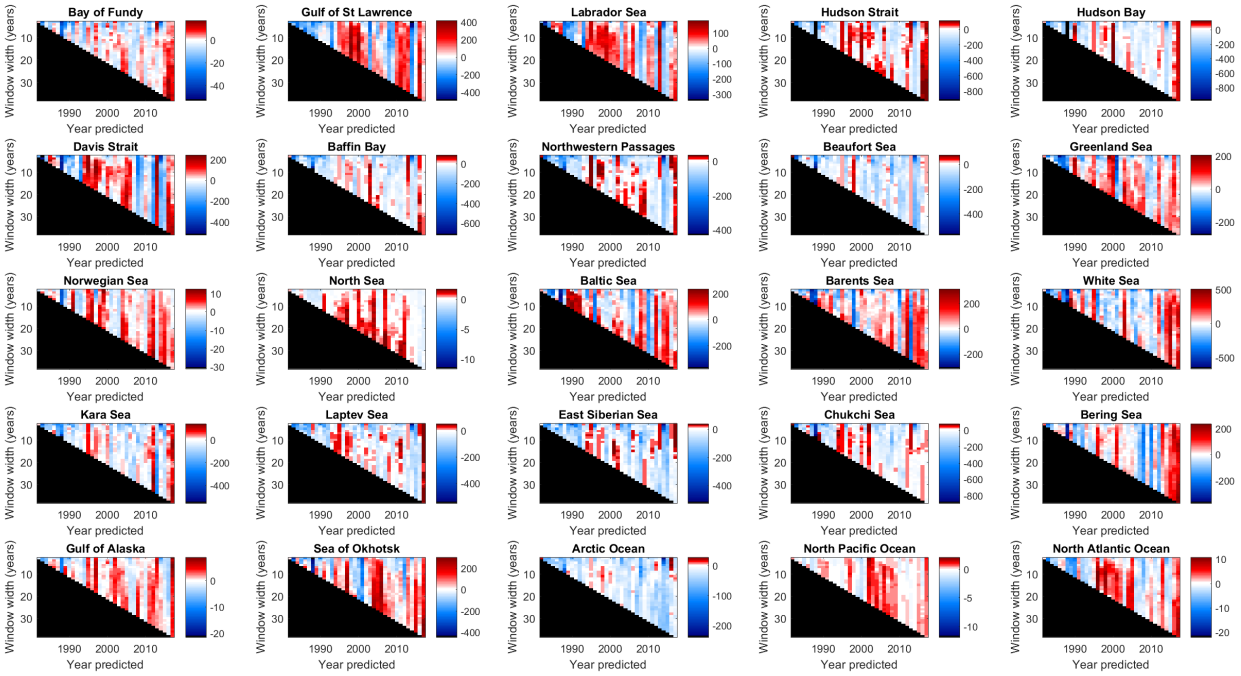


Figure 38: Sea ice concentration prediction error for the northern hemisphere regions for the month of March, when the maximum sea ice concentration occurs. Greater window widths generally produce better predictions, but the specifics vary between regions.

## Personnel Supported

Dr. Maria Fonoberova, Dr. Igor Mezic, Dr. James Hogg

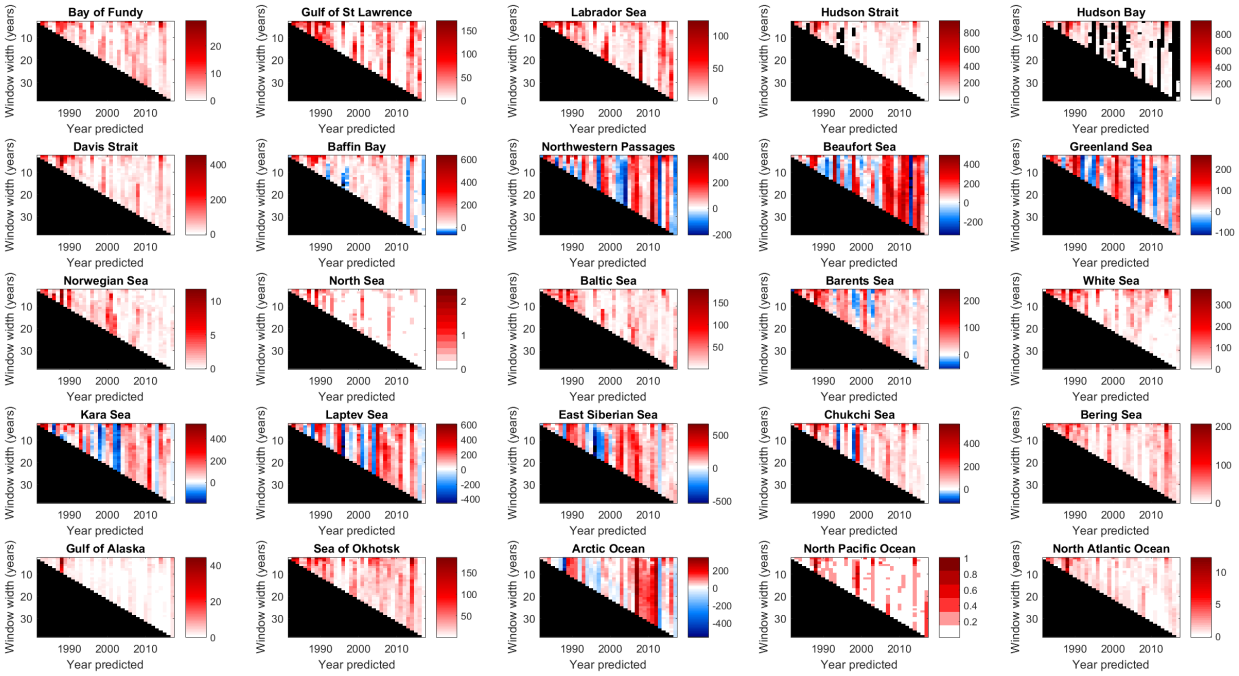


Figure 39: Sea ice concentration prediction error for the northern hemisphere regions for the month of September, when the minimum sea ice concentration occurs. As for the March case, greater window widths generally produce better predictions, but the specifics vary between regions.

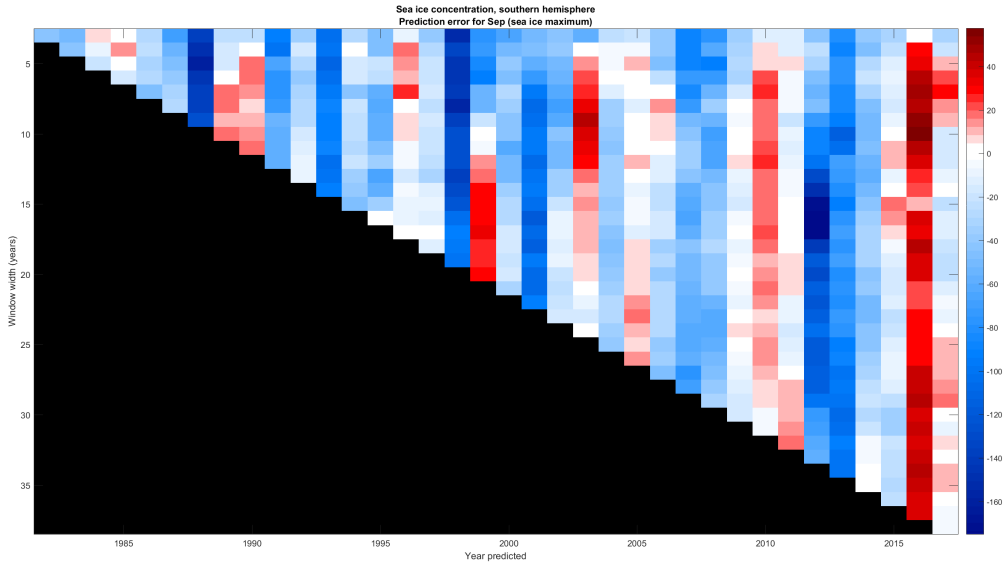


Figure 40: Sea ice concentration prediction error for the entire southern hemisphere region covered by the available satellite data, for the month of September, when the maximum sea ice concentration occurs.

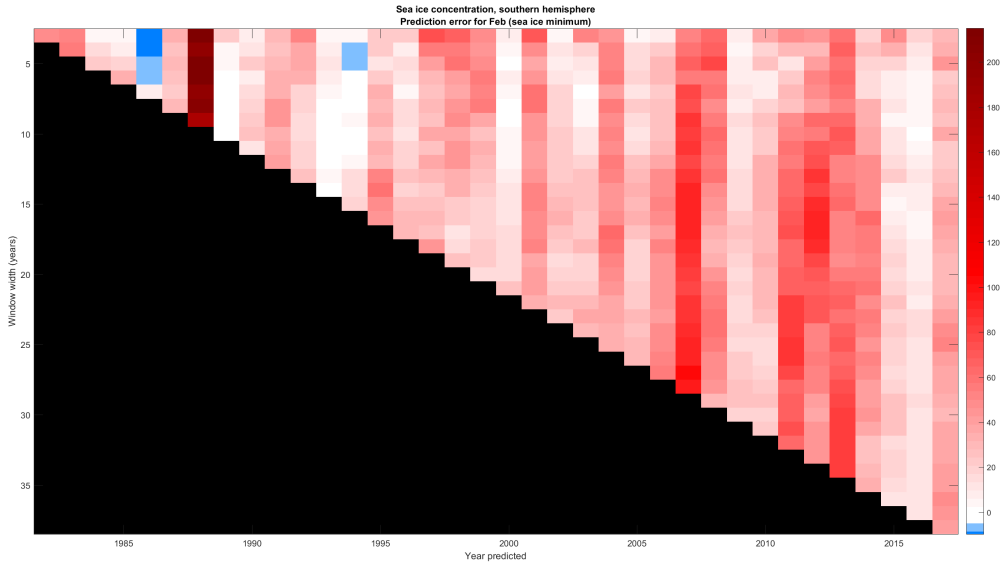


Figure 41: Sea ice concentration prediction error for the entire southern hemisphere region covered by the available satellite data, for the month of February, when the minimum sea ice concentration occurs. Here, longer windows do not as often produce better prediction results.

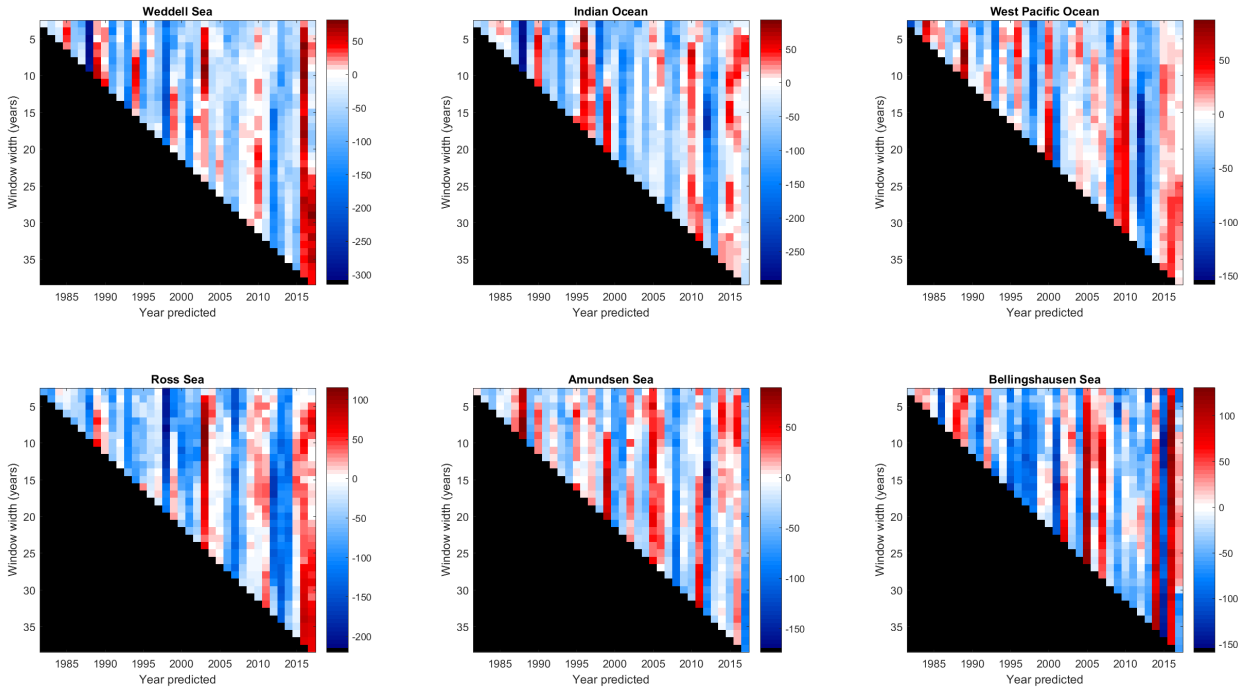


Figure 42: Sea ice concentration prediction error for the southern hemisphere regions for the month of September, when the maximum sea ice concentration occurs.

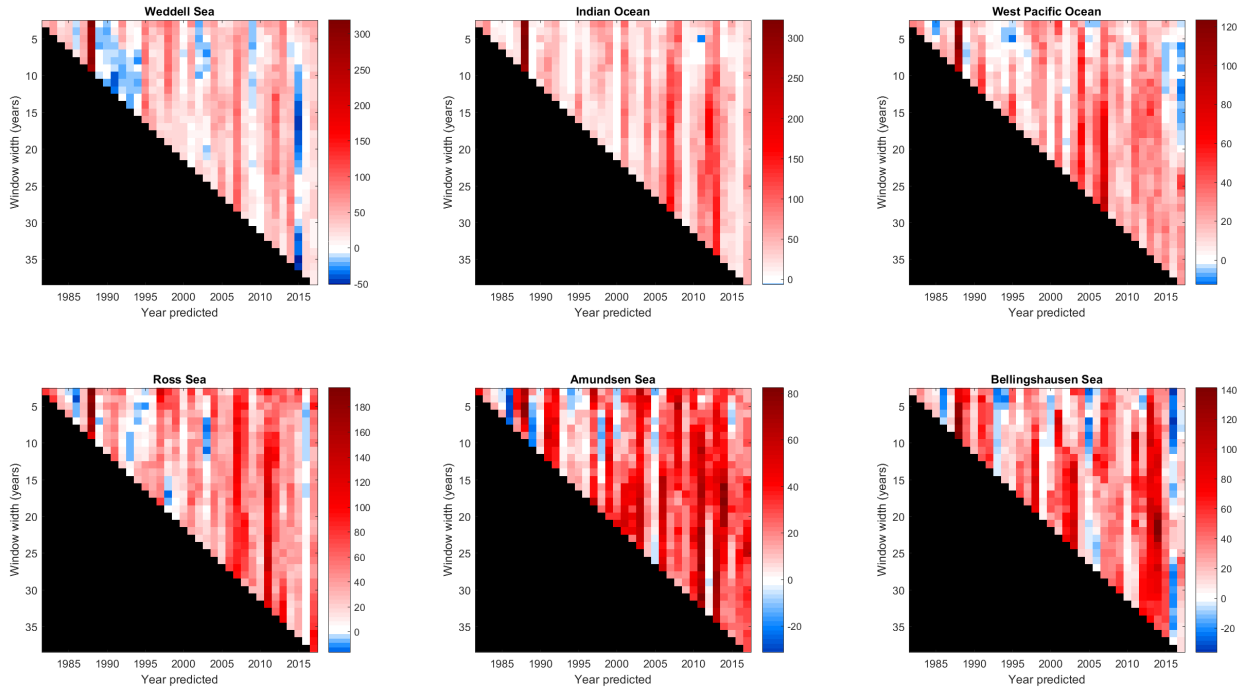


Figure 43: Sea ice concentration prediction error for the southern hemisphere regions for the month of February, when the maximum sea ice concentration occurs.